




## Drivers of Warming in Lake Nam Co on Tibetan Plateau Over the Past 40 Years

Yi Shi<sup>1,2</sup>, Anning Huang<sup>1,2</sup> , Weiqiang Ma<sup>3</sup> , Lijuan Wen<sup>4</sup> , La Zhu<sup>5</sup>, Xianyu Yang<sup>6</sup>, Yang Wu<sup>1,2</sup>, and Chunlei Gu<sup>1,2</sup>

<sup>1</sup>CMA-NJU Joint Laboratory for Climate Prediction Studies, School of Atmospheric Sciences, Nanjing University, Nanjing, China, <sup>2</sup>Frontiers Science Center for Critical Earth Material Cycling, Nanjing University, Nanjing, China, <sup>3</sup>Key Laboratory of Tibetan Environment Changes and Land Surface Processes, Institute of Tibetan Plateau Research, Chinese Academy of Sciences, Beijing, China, <sup>4</sup>Key Laboratory of Land Surface Process and Climate Change in Cold and Arid Regions, Chinese Academy of Sciences, Lanzhou, China, <sup>5</sup>College of Science, Tibet University, Lhasa, China, <sup>6</sup>College of Atmospheric Sciences/Plateau Atmosphere and Environment Key Laboratory of Sichuan Province, Chengdu University of Information Technology, Chengdu, China

### Key Points:

- As an ice-covered lake, Lake Nam Co (LNC) warmed with a smaller rate than the local surface air temperature during 1980–2018
- The interdecadal shift of surface specific humidity played a key role in the hiatus of LNC warming after 1997
- The individual and cross contributions of different atmospheric factors to the long-term trend of surface water temperature are quantified

### Correspondence to:

A. Huang,  
[anhuang@nju.edu.cn](mailto:anhuang@nju.edu.cn)

### Citation:

Shi, Y., Huang, A., Ma, W., Wen, L., Zhu, L., Yang, X., et al. (2022). Drivers of warming in Lake Nam Co on Tibetan Plateau over the past 40 years. *Journal of Geophysical Research: Atmospheres*, 127, e2021JD036320. <https://doi.org/10.1029/2021JD036320>

Received 6 DEC 2021  
 Accepted 18 JUL 2022

### Author Contributions:

**Conceptualization:** Anning Huang, Weiqiang Ma  
**Data curation:** Yi Shi, La Zhu, Yang Wu, Chunlei Gu  
**Formal analysis:** Yi Shi, Xianyu Yang  
**Funding acquisition:** Anning Huang, Lijuan Wen, Xianyu Yang  
**Investigation:** Yi Shi, Lijuan Wen, Chunlei Gu  
**Methodology:** Yi Shi, Anning Huang, Yang Wu  
**Resources:** Yi Shi, Lijuan Wen  
**Software:** Yi Shi  
**Supervision:** Anning Huang, Weiqiang Ma  
**Validation:** Yi Shi  
**Visualization:** Yi Shi  
**Writing – original draft:** Yi Shi, Yang Wu  
**Writing – review & editing:** Anning Huang, Weiqiang Ma, Lijuan Wen, La Zhu, Xianyu Yang

**Abstract** The lake surface water temperature (LSWT) on Tibetan Plateau (TP) is sensitive to climate change. Based on a 1-D lake model, we have investigated the interdecadal variation and long-term trend of LSWT in Lake Nam Co (LNC) on TP during 1980–2018 and quantified the relative contributions of atmospheric factors to the LSWT trend. Results show LNC was warmed with a rate of 0.29°C decade<sup>-1</sup>, which is smaller than the warming of ambient air (0.45°C decade<sup>-1</sup>). The weakened wind speed, rising air temperature, increased downward longwave radiation, and decreased shortwave radiation contributed about 35%, 30%, 20%, and –15% of the estimated long-term LSWT trend during 1980–2018, respectively. The contribution rate of 32.5% was from the interactions among all forcing variables. The primary warming was completed before 1997 (0.30°C decade<sup>-1</sup>) and was followed by a hiatus that the LSWT jumped to a warm level with a slightly negative trend (–0.08°C decade<sup>-1</sup>) after 1997. During this hiatus, the wind speed recovered from decrease and the deceleratingly increased downward longwave radiation slowed down the LNC warming. Particularly, the specific humidity shifted from increasing to decreasing trend played a key role in the hiatus of LNC warming after 1997, despite its slight contribution (–2.5%) to the LSWT trend during 1980–2018. The results showed the particularity of warming for a TP lake compared to the other ice-covered lakes worldwide and provided a quantitative perspective for understanding the relative contributions of atmospheric factors to the long-term trend of LSWT.

## 1. Introduction

As “the world water tower” (Xu et al., 2008), Tibetan Plateau (TP) is dotted with more than 1400 inland lakes with an area of over 1 km<sup>2</sup> (Zhang et al., 2019), most of which are salt lakes (Liu et al., 2021). The total lake area on the TP exceeds 50,000 km<sup>2</sup> in 2018, which accounts for around 57% of the total lake area in China (Tao et al., 2020). The unstable boundary layer of TP lakes (Wang, Ma, et al., 2015; Wen et al., 2016) causes huge amounts of water and heat transported into the middle atmosphere (Lazhu et al., 2016; Wang, Ma, et al., 2020), which directly affects the local weather and climate in the TP (Wen et al., 2015; Wu, Huang, et al., 2019). In turn, lakes on the TP are also sensitive to climate change because of the distinct alpine climate (Yang et al., 2014; Zhang et al., 2020). Due to the sparse population of TP, the changes in TP lakes are more reflective of natural climate change than the lakes affected directly by human behavior (Pekel et al., 2016; Yang et al., 2020; Zhang et al., 2017).

The direct response of a lake to climate warming is the rising lake surface water temperature (LSWT), which would further influence aquatic systems in various aspects (Adrian et al., 2009; Shimoda et al., 2011; Woolway et al., 2021). Rising LSWT could enhance and prolong thermal stratification (Anderson et al., 2021; Kraemer et al., 2015) and reduce the ice duration in seasonally ice-covered lakes (Kropáček et al., 2013; Sharma et al., 2019), thereby enhancing surface evaporation (Lazhu et al., 2016) and altering lake mixing regimes (Woolway & Merchant, 2019). Additionally, warming of lakes also causes lake ecosystems degradation (Cohen et al., 2016; Snorheim et al., 2017) and promotes greenhouse gas emissions in lakes (Mu et al., 2016; Tranvik et al., 2009;

F. Yan et al., 2018). Thus, it is necessary to understand how the lake temperatures respond to climate change for better prediction and reasonable socioeconomic countermeasures.

Global satellite and in situ comprehensive analyses about LSWT demonstrate that lakes have been warming worldwide in summer (O'Reilly et al., 2015; Schneider & Hook, 2010), with a mean increasing rate of 0.34°C per decade from 1985 to 2009. The most evident rises of LSWT appear in middle- and high-latitude of the northern hemisphere, even exceeding local surface air temperatures, such as the Great Lakes (Austin & Colman, 2007; Huang et al., 2012; Schneider & Hook, 2010) and Nordic Lakes (Livingstone & Padišák, 2007; Niedrist et al., 2018). The increase of LSWT is mainly attributed to surface air warming (Piccolroaz et al., 2013; Schmid et al., 2014; Schneider & Hook, 2010) and further to anthropogenic climate change (Grant et al., 2021). Other meteorological factors were emphasized recently, such as increased radiation (Fink et al., 2014; Schmid & Köster, 2016) and reduced wind speed (Huang et al., 2012; Woolway et al., 2019). Meanwhile, changes in LSWT are of heterogeneity globally (O'Reilly et al., 2015) but coherence regionally (Livingstone & Padišák, 2007), which reflect the role of background climate, thermal conditions of lakes, local geographic and geomorphic features including lake elevation (Livingstone et al., 2005), morphology (Kraemer et al., 2015; Magee & Wu, 2017), depth (Kraemer et al., 2015), and water clarity (Rose et al., 2016; Subin et al., 2012). For instance, lakes covered with ice typically warm faster than ambient air temperatures, and lake morphology influences the strength of this response (Austin & Colman, 2007; Butcher et al., 2015).

Relative to other regions, the thermal response of TP lakes to climate change is of distinctive research importance, because of the unique geological environment (e.g., high elevation, lots of salt and glacier-fed lakes; Zhang et al., 2020), alpine climate (e.g., low air temperature but high solar radiation) and climate change characteristics (e.g., higher warming rate than the global mean; Duan & Xiao, 2015; Kuang & Jiao, 2016). It is due to these features that TP lakes are often excluded from some analyses about LSWT on a global scale (Layden et al., 2015; Schmid et al., 2014; Woolway & Merchant, 2017).

Owing to the field observations limited by the remoteness and wilderness, many studies on TP lakes rely more on satellites. Zhang et al. (2014) first retrieved the night land surface temperature (LST) from Moderate Resolution Imaging Spectroradiometer (MODIS/Terra) during 2001–2012 to study the LSWT of 52 lakes with an area of more than 50 km<sup>2</sup> on TP, 31 lakes (60%) of which showed an increasing temperature trend. Yet another similar survey from 2001 to 2015 showed that only 18 (32%) of the lakes warmed in the daytime and 27 (48%) at nighttime (Song et al., 2016). If the perspective was widened to 374 lakes ( $\geq 10$  km<sup>2</sup> each), the majority of lakes (70%) showed warming (Wan et al., 2018). It implies that there are large uncertainties in LSWT trends within the time span of the satellite data at present, such as MODIS since 2000 to present, Landsat-7 since 1999, the Advanced Along Track Scanning Radiometer (ATSR/AATSR) series since 1995, and Advanced Very High Resolution Radiometer (NOAA-AVHRR) since 1981 (Tomlinson et al., 2011).

Besides, there are shortcomings of lower sampling density in earlier years (e.g., AVHRR and AATSR) and sampling discontinuities due to cloud pollution especially local frequent convection in TP (Lazhu et al., 2016; Rao et al., 2019; Wu, Huang, et al., 2019), which pose problems for studying the interannual variability and long-term trends when using statistic methods. These shortcomings could be compensated by numerical models with solid physical processes, and more importantly, numerical experiments could be designed to decompose the contributions of different atmospheric forcings on the lake system.

1-D numerical simulation of lakes has been widely used to study long-term changes in lakes (Anyah & Semazzi, 2004; Magee et al., 2016; Perroud et al., 2009; Woolway & Merchant, 2019). In recent years, LSWT trends over 30 years have been successfully obtained in several large lakes on TP. Huang et al. (2017) indicated that the lake surface warming in Lake Nam Co during 1979–2012 was dominated by the increased surface air temperature and enhanced downward longwave radiation. Besides these two factors, Su et al. (2019) found that the weakened surface wind speed also contributes to the warming in Qinghai Lake. While the decrease of solar radiation may offset the warming effect of surface air temperature, such as in Lake Ngoring and Lake Gyaring (Kirillin et al., 2017). In the context of similar climate change, however, these lakes show different impact factors affecting the lake temperature. Hence it is necessary to comprehensively examine the contributions of different atmospheric factors to the LSWT variation over TP lakes.

In this study, we focus on Lake Nam Co (LNC), the third largest lake in the TP, using a 1-D lake model WRF-Lake (Huang et al., 2019; Xu et al., 2016) to investigate: the interdecadal variation and long-term trend of LSWT in

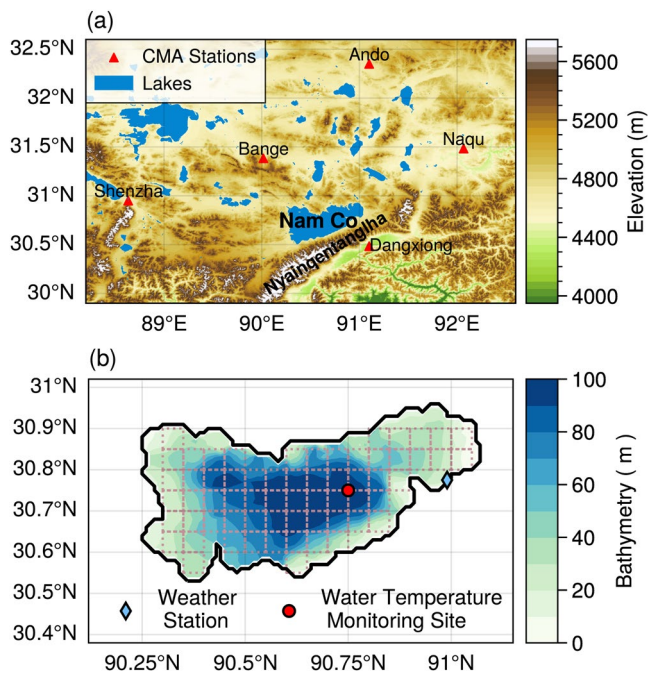


**Figure 1.** Topography around Lake Nam Co (LNC) and the locations of China Meteorological Administration (CMA) stations (a). Bathymetry of LNC and the locations of the weather station and water temperature monitoring site; the dashed grids indicate the model grids (b).

LNC over the last 40 years (1979–2018); the relative contributions of different atmospheric factors to the long-term trend of LSWT. This study can improve our understanding of the impact of climate changes on the thermal conditions of lakes in alpine regions and provide a reference for prediction and countermeasures of future changes in TP lakes.

## 2. Material and Methods

### 2.1. Study Area

LNC, the highest large lake in China (4,718 m a.s.l) with a surface area over 2,000 km<sup>2</sup> (Lazhu et al., 2016), is situated in the Central Tibetan Plateau (30°30′–30°55′N, 90°16′–91°03′E), and north to the Nyainqentanglha Mountains (Figure 1a). The maximum and mean depth of LNC exceed 90 and 50 m (Figure 1b). It is an endorheic and therefore a brackish lake with a salinity of around 1.7 g L<sup>-1</sup> (Wang et al., 2006), which affects the temperature at the maximum density ( $T_{d_{max}}$ ) and freezing point of lake water (Lazhu et al., 2021).

The Nam Co basin is influenced by the alpine climate. According to the weather station observations on the southeastern shore of LNC during 2006–2018 (Figure 1b; Wang & Wu, 2018, 2019), the multi-year annual mean surface air temperature, pressure, solar radiation are  $-0.4^{\circ}\text{C}$ , 571.2 hPa, 245.0 W m<sup>-2</sup>, respectively. The multi-year annual mean 10 m wind speed in the region is 3.4 m s<sup>-1</sup>, with the highest of 4.5 m s<sup>-1</sup> in January due to the westerly system (Wang, Ma, et al., 2020). The multi-year annual mean relative humidity is 57.1% with a peak of 68.6% in August. The mean annual precipitation is around 380.0 mm, most of which is concentrated between

May and October controlled by the southwestern monsoon, and it is an important source of recharge for LNC (Zhu et al., 2010).

### 2.2. Datasets and Processing

#### 2.2.1. Meteorological Data and Corrections

The China Meteorological Forcing Data set (CMFD) (Yang & He, 2019) during 1979–2018 was used to drive the WRF-Lake model. It has been proven of better reliability for TP lakes compared to other reanalysis datasets, such as ERA-Interim and NCEP/NCAR (Du et al., 2019). The CMFD has a temporal resolution of 3 hrs and a spatial resolution of 0.1°. It includes seven meteorological elements: surface air temperature (SAT) at 2 m above ground, surface pressure (SP), and surface specific humidity (SSH), 10 m wind speed (WS), downward shortwave radiation ( $SW_{\downarrow}$ ), downward longwave radiation ( $LW_{\downarrow}$ ) at the surface, and precipitation rate (PR). More information can be found in the paper of He et al. (2020) and available at <https://data.tpdc.ac.cn/en/data/8028b944-daaa-4511-8769-965612652c49/>. All variables were interpolated into the lake model grids with a resolution of 0.05° by the bilinear interpolation method (Peng et al., 2019).

In this study, we found an unusually positive anomaly (relative to climatic state) of LSWT during 1993–2003 but it was normal in the following years (not shown). This time-varying error should be dependent on the forcing data rather than the model. It could be further attributed to the anomalies of WS and SSH during this period. To correct the long-term variation of each atmospheric forcing, we replaced the daily CMFD data with the arithmetic average of five China Meteorological Administration (CMA) stations around LNC (Figure 1a; Wu & Zhu, 2008) without  $SW_{\downarrow}$  and  $LW_{\downarrow}$ . For the consistency of data quality over time, the above replacement was taken for all years (1979–2018).

Due to the large difference in elevation among these five CMA stations, thermodynamic variables must be calibrated to the elevation ( $Z_N = 4,730$  m) of Nam Co station. The surface air temperature ( $T$ , units: K) and pressure ( $P$ , units: hPa) at an elevation of  $Z$  (m) were calibrated using the following formulas (Hafner & Smith, 1985):

$$P' = P \left( \frac{T}{T + \gamma \cdot (Z_N - Z)} \right)^{\frac{g}{R\gamma}} \quad (1)$$

$$T' = T - \gamma \cdot (Z_N - Z) \quad (2)$$

where  $g = 9.81$  m s<sup>-2</sup>,  $\gamma = 0.007$  K m<sup>-1</sup>, and  $R = 287$  J K<sup>-1</sup> kg<sup>-1</sup>.  $T'$  and  $P'$  are calibrated temperature and pressure, which were further used to calculate the surface specific humidity (SSH, kg kg<sup>-1</sup>) by an empirical formula (Bolton, 1980; Murray, 1967):

$$\text{SSH} = \text{RH} \times 0.622 \times \frac{es}{P'} = \frac{\text{RH} \times 0.622}{P'} \times \begin{cases} 6.1078 \exp \left[ \frac{17.27(T' - 273.16)}{T' - 35.86} \right], & T' \geq 0 \\ 6.112 \exp \left[ \frac{17.67(T' - 273.16)}{T' - 29.66} \right], & T' < 0 \end{cases} \quad (3)$$

where RH is the relative humidity (%),  $es$  is the saturation vapor pressure (hPa). The corrected data above are noted as C-CMFD.

Nevertheless, these distant land sites from LNC are hardly a true reflection of the physical information over the lake area, so we further adjusted the C-CMFD derived above using the daily data from the weather station on the southeastern shore of LNC during 2006–2018 (Wang & Wu, 2018, 2019). The SAT, RH, SP, WS, and SW<sub>1</sub> were used in this data set; LW<sub>1</sub> during 2005–2016 was accessible from Ma (2020), a data set of hourly land-atmosphere interaction in situ observations (Ma et al., 2020); SSH over the water surface was calculated by Equation 3.

Following Lazhu et al. (2016) and Huang et al. (2017), we established the linear relationship between the C-CMFD and data from the Nam Co station for adjustment, where only the data points above the fifth percentile (twentieth for LW<sub>1</sub>) of the Gaussian kernel density were used to calculate. As shown in Figure 2, except for the WS and LW<sub>1</sub>, the variables of C-CMFD show a good consistency with the field observation at Nam Co station with a small mean bias and root mean square error (RMSE). The linear adjustment based on regression equations in Figure 2 resulted in a significant reduction in mean bias but little reduction in RMSE.

Finally, there was still an underestimation of the WS over the lake using data measured on the lakeshore. We multiplied by a constant scaling factor of 1.29 for WS (Schmid & Köster, 2016). The scaling factor was roughly calculated from the wind observation by B. Wang et al. (2019), with 3.65 m s<sup>-1</sup> in the small lake next to LNC and 4.71 m s<sup>-1</sup> in LNC from July to November in 2015 and 2016.

Above correction and adjustment were not performed for precipitation, since the precipitation rate in CMFD has merged satellite data like the Tropical Rainfall Measuring Mission (TRMM) data set and was considered more reliable over lake relative to the data from land sites (He et al., 2020; Wu, Guo, et al., 2019).

### 2.2.2. Lake Data and Satellite Data

The bathymetry of LNC (Wang et al., 2009) was adopted in the WRF-Lake model (Figure 1b). To validate the simulation results, we used the daily lake water temperature profile data at the depths of 3, 6, 16, 21, 26, 31, and 36 m (Wang, 2020). It was recorded by the monitoring site in the southeast of LNC (30°45.74'N, 90°46.83'E; Figure 1b; J. Wang et al., 2019, 2020) from 1 January 2012 to 31 December 2013.

To evaluate the water temperatures on the lake surface, we used Land Surface Temperature (LST) products MOD11A1 (Wan et al., 2015a) and MOD11A2 (Wan et al., 2015b) from Moderate Resolution Imaging Spectroradiometer (MODIS/Terra) during 2001–2018, available at [https://lpdaac.usgs.gov/product\\_search/?query=MOD11%26view=cards%26sort=title](https://lpdaac.usgs.gov/product_search/?query=MOD11%26view=cards%26sort=title). The MOD11A1 includes two instantaneous observations at 10:30 and 22:30 local time every day with a resolution of 1 km, and the average of these two observations was compared to the average of the simulation results at the corresponding time. The MOD11A2 provides 8-day averaged LSTs derived from MOD11A1 to estimate linear trends of LSWT (Song et al., 2016; Zhang et al., 2014; Zhao

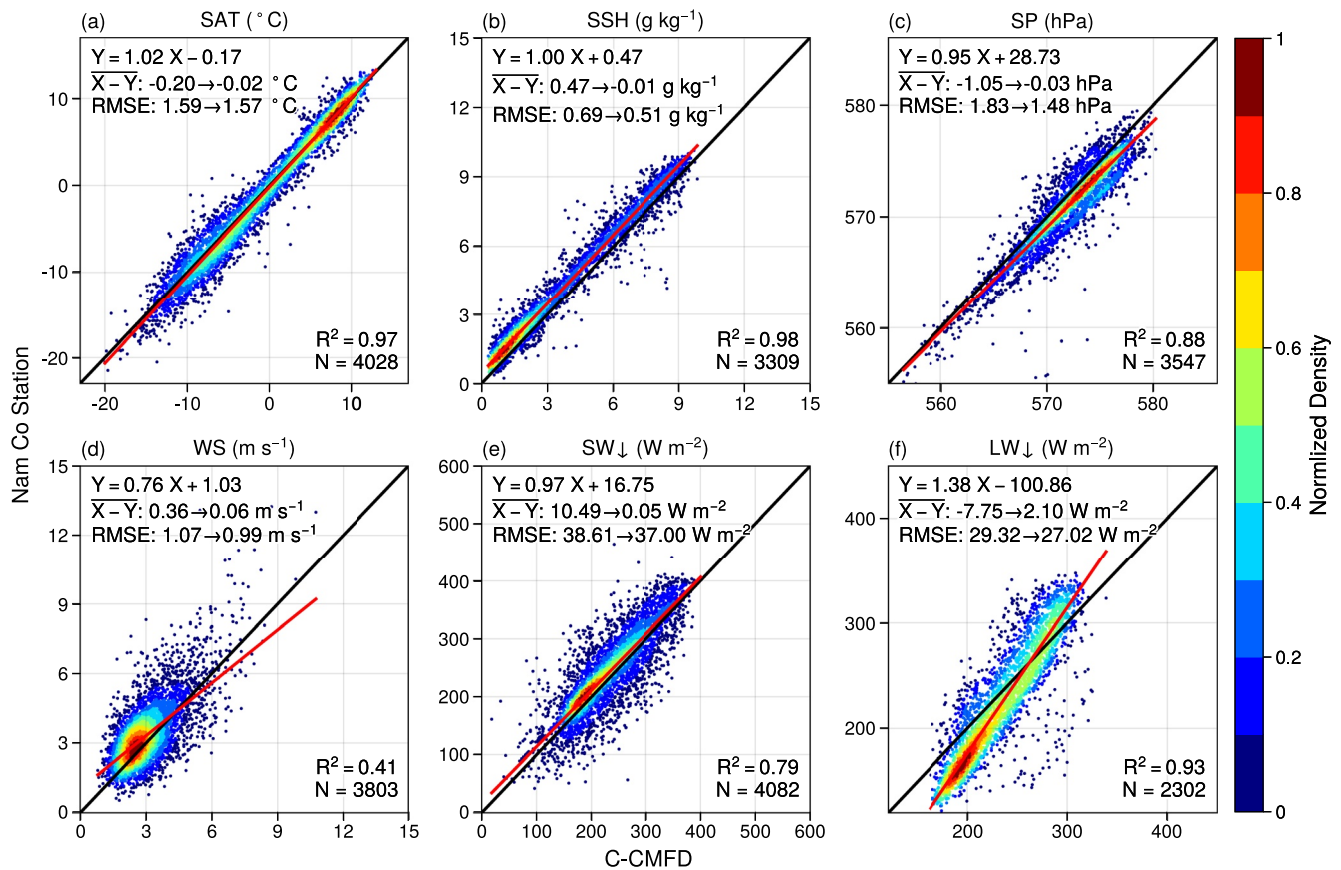


**Figure 2.** Linear regression of the observation at Nam Co station (Y-axis) with respect to C-China Meteorological Forcing Data set (CMFD) (X-axis): (a) surface air temperature (SAT), (b) surface specific humidity (SSH), (c) surface pressure (SP), (d) 10 m wind speed (WS), (e) downward shortwave radiation ( $SW_{\downarrow}$ ), and (f) downward longwave radiation ( $LW_{\downarrow}$ ).  $\bar{X} - \bar{Y}$  is the mean bias of C-CMFD compared to Nam Co station observation and N is the number of samples. The right arrows in  $\bar{X} - \bar{Y}$  and root mean square error indicate the changes in their values before and after linear adjustment. The color of scatters represents the normalized Gaussian kernel density, and the larger values indicate more points around.

et al., 2020). The obvious outliers have been removed, and the missing values in MOD11A2 were filled by linear interpolation in the time dimension. All data for each time sample were interpolated onto the model grids by sub-grids averaging.

We also utilized GloboLakes LSWT Data set including daily averaged LSWTs with a resolution of 0.05° (Carrea & Merchant, 2019; Politi et al., 2016) to evaluate the modeled LSWT trends over a longer time range (1996–2018). This data set has been also extensively evaluated and validated using in-situ observations (MacCallum & Merchant, 2012; Zhang et al., 2021; Zhao et al., 2020). GloboLakes LSWT Data set includes data from 1 June 1995–31 December 2016, and the data after 2017 can be downloaded from Copernicus Climate Data Store (<https://cds.climate.copernicus.eu/cdsapp#!/dataset/10.24381/cds.d36187ac?tab=overview>).

Note that, we have removed the grids (not shown in Figure 1b) near the lake shoreline that may affect our analysis both in model results and satellite data.

### 2.3. Model Description

The WRF-Lake Model is a 1-D mass and energy balance lake model based on the Community Land Model version 3.5, which originated from the eddy diffusion model developed by Henderson-Sellers (1985) and Hostetler and Bartlein (1990), then further was developed by Subin et al. (2012) and Gu et al. (2015). The model is discretized to solve for the temperature on different layers, including 10 or 25 layers of water and ice (25 used here), up to 5 layers of snow on the lake ice, and 10 layers of soil at the lake bottom (Gu et al., 2015; Huang et al., 2019; Subin et al., 2012; Wu et al., 2020).

**Table 1**  
*Experimental Design*

Experiments	Forcing data
CTRL-2D	Adjusted C-CMFD over independent model grids with actual lake depths (Figure 1b)
CTRL-1D	Regional averaged adjusted C-CMFD over LNC as a single point with the mean lake depth of 50 m
EXP-F	Based on CTRL-1D, a series of perturbations were added separately on the climatic mean of each forcing variable
EXP-Z	Based on CTRL-1D, but the forcing data were decorrelated on an interannual scale in each month

The model was developed for shallow freshwater lakes originally and inapplicable to deep and brackish lakes like LNC (Fang et al., 2017). Huang et al. (2019) and Wu et al. (2020) improved the WRF-Lake model for TP lakes by replacing the constant surface roughness lengths with a parameterized scheme, increasing the turbulent mixing, decreasing the light extinction coefficient, and adjusting  $Td_{\max}$  (for details, see Huang et al., 2019; Subin et al., 2012; Wu et al., 2020).

At the lake surface layer, the energy balance needs to be satisfied (Subin et al., 2012):

$$\beta(1 - \alpha)SW_{\downarrow} + (LW_{\downarrow} - \varepsilon\sigma T_s^4) - SH_{\uparrow} - LH_{\uparrow} = G_{\downarrow} \quad (4)$$

where  $\alpha$  is the lake surface albedo to the shortwave radiation  $SW_{\downarrow}$  ( $\text{W m}^{-2}$ ) and  $\beta$  is the absorption rate of the net shortwave radiation by lake surface ( $\beta = 0.2$  for the water depth  $>4$  m). The term  $LW_{\downarrow} - \varepsilon\sigma T_s^4$  is net downward longwave radiation with the lake surface emissivity  $\varepsilon = 0.97$  and  $\sigma = 5.67 \times 10^{-8} \text{ W m}^{-2} \text{ K}^{-4}$ .  $LW_{\downarrow}$  is downward longwave radiation ( $\text{W m}^{-2}$ ), and  $T_s$  (K) is the water temperature at the lake surface.  $SH_{\uparrow}$  and  $LH_{\uparrow}$  are upward sensible and latent heat fluxes ( $\text{W m}^{-2}$ ), respectively, and  $G_{\downarrow}$  represents downward heat flux ( $\text{W m}^{-2}$ ) from the surface layer into the lake.

The controlled equation of the thermal diffusion model in the water body is given by

$$\frac{\partial T}{\partial t} = \frac{\partial}{\partial z} \left[ (k_m + m_d k_e) \frac{\partial T}{\partial z} \right] - \frac{1}{c_w} \frac{d\Phi}{dz} \quad (5)$$

where  $T$  is water temperature (K) at depth  $z$  (m).  $t$  is time (s) and  $c_w$  is the volumetric heat capacity ( $\text{J m}^{-3} \text{ K}^{-1}$ ).  $k_m$  is the molecular diffusion coefficient ( $\text{m}^2 \text{ s}^{-1}$ ), and  $k_e$  is the wind-driven eddy diffusion coefficient ( $\text{m}^2 \text{ s}^{-1}$ ).  $m_d = \begin{cases} 0, & z < 25 \text{ m} \\ 60, & z \geq 25 \text{ m} \end{cases}$  is an enhanced mixing factor of  $k_e$  to compensate for the mixing effect caused by certain physical processes that the model fails to describe (Subin et al., 2012; Wu et al., 2020).  $\Phi = (1 - \beta)(1 - \alpha)SW_{\downarrow}e^{-\eta \max(z-z_0, 0)}$  is the shortwave radiation ( $\text{W m}^{-2}$ ) penetrating into the depth  $z$ . And  $z_0 = 0.6$  m is the minimum depth where no additional absorbed shortwave radiation. The light extinction coefficient  $\eta$  was set to a constant of  $0.1 \text{ m}^{-1}$  close to the observation (Wang et al., 2009). Additionally,  $Td_{\max}$  is also a vital parameter related to the mixing and freeze-thaw processes, and it was set to  $3.6^\circ\text{C}$  (Lazhu et al., 2021).

## 2.4. Experimental Design and Analysis

The WRF-Lake model was driven by the adjusted C-CMFD and integrated continuously from 1 June 1979 to 31 December 2018 with a time step of 10 min, where the forcing data were also interpolated linearly to every 10 min. The running in 1979 was for spin-up so not analyzed. For a simple initial condition, we ran the model starting from a state where the lake is fully mixed vertically with a temperature of  $3.5^\circ\text{C}$ . These settings were applied to the offline experiments listed in Table 1.

The CTRL-2D was simulated over independent model grids to analyze the interdecadal variation and long-term trend of LSWT in LNC over 1980–2018, and the results were regionally averaged over the lake to mitigate the effect of intralake heterogeneity (Woolway & Merchant, 2018). As a base for subsequent sensitivity experiments, CTRL-1D was simulated at a single point for efficiency, and its results should have a similar long-term trend and interannual variations to CTRL-2D.

#### 2.4.1. Changing the Climatic Mean Atmospheric Forcing Variables

To investigate how the climatic perturbations of each forcing variable affect LSWT over the climatic mean state, we performed a set of experiments (EXP-F) for each forcing variable using the change factor approach that is traditionally utilized to analyze the sensitivity of a system to climate change (Butcher et al., 2015; Magee & Wu, 2017). Given a forcing variable, we first calculated its standard deviation  $\sigma_m$  monthly ( $m = 1, 2, \dots, 12$ ), and then added respective perturbation  $\lambda_n \sigma_m$  to the base value for each month in all years with other variables unchanged. Here  $\lambda_n$  varied from  $-3.0$  to  $3.0$  with equally spaced increments of  $0.2$  and so there are 31 sample experiments ( $n = 1, 2, \dots, 31$ ). In particular, the experiment with  $\lambda_n = 0$  was identical to the control experiment (CTRL-1D), that is, there was no change for all forcing variables.

It should be noted that the perturbation ranges were not selected subjectively but based on the variation characteristics of the variables themselves, so the actual climatic extremes are covered conservatively and avoid unrealistic scenarios (Stetler et al., 2021). Additionally, it has been proven that each experiment retains the same interannual variability and long-term trend.

Based on the above experiments, a climatic mean series  $\overline{LSWT}(\bar{F})$  can be obtained by calculating climatic means for the set of experiments corresponding to a given forcing variable  $F$ , where the overbar symbol denotes the climatic state. We can define the absolute sensitivity  $S_a$  of LSWT response to each atmospheric forcing variable  $F$ , where  $S_a = \partial \overline{LSWT} / \partial \bar{F}$ . Furthermore, because the  $n$ th experiments with the same  $\lambda_n$  have the same magnitude of climate perturbation for all variables, we can also define relative sensitivity  $S_r$  to compare the relative magnitude that LSWT responds to each forcing variable under per unit standard deviation of climate perturbation. Here  $S_r = \sigma S_a$ , and  $\sigma$  is the annual mean standard deviation of a given forcing variable.

#### 2.4.2. Estimating the Contributions of Forcing Variables to the LSWT Trend

In this study, a method based on partial derivatives (Equation 6) was used to estimate the contributions of atmospheric forcing variables to the LSWT trend of LNC. This method has been widely applied to evaluate the contributions of climatic factors to hydrological or ecological changes (Roderick et al., 2007; Wang, Wang, et al., 2015; Y. Yan et al., 2019). This approach assumes that on the first order (long-term scale), the trend of LSWT (i.e.,  $dLSWT/dt$ ) should respond linearly to the changes of forcing variables (Austin & Colman, 2007):

$$\left( \frac{dLSWT}{dt} \right)_F \approx \sum_i \frac{\partial LSWT}{\partial F_i} \frac{dF_i}{dt} \approx \sum_i S_{a_i} \frac{dF_i}{dt} \quad (6)$$

Accordingly, we could quantify the contribution of each forcing variable  $F_i$  to the trend of LSWT based on absolute sensitivities  $S_{a_i}$  and the trend of forcing variables  $dF_i/dt$ .

Note that, Equation 6 implies two assumptions: first,  $S_{a_i}$  is a constant that is,  $\overline{LSWT}(\bar{F}_i)$  varies linearly; second, the interannual change in LSWT resulted from one forcing variable  $F_i$  approximately equals the climatic response of LSWT to the variable, that is,  $\partial LSWT / \partial F_i \approx S_{a_i}$ .

However, the changes (i.e.,  $dF_i/dt$ ) in forcing variables are influenced by their interactions, which may confound their individual contributions to the trend of LSWT. These interactions are expressed as the collinearity among forcing variables on an interannual scale, which originates from the strong coupling of the climate system.

To eliminate the effect of interactions as much as possible, we used zero-phase component analysis (ZCA) to decorrelate the forcing variables (i.e., to reduce the linear correlation among different forcing variables) for each month. This method is commonly used for data pre-processing in machine learning and is also applied to the reconstruction of climate fields (Bocinsky & Kohler, 2014). Specifically, the standardized anomaly matrix  $F_{p \times s}^*$  with  $p$  forcing variables and  $s$  times are calculated first. Each row  $F_i^* = F_i - \bar{F}_i / \sigma_i$  of the matrix  $F^*$  representing a forcing variable, where  $\bar{F}_i$  is the mean value (i.e., climatic state) and  $\sigma_i$  is the standard deviation. Then we take a linear transform  $W$  on  $F^*$ :

$$\mathbf{Z}^* = \mathbf{W}\mathbf{F}^* = \left(\mathbf{U}\mathbf{\Lambda}^{-\frac{1}{2}}\mathbf{U}^T\right)\mathbf{F}^* \quad (7)$$

where  $\mathbf{W} = \mathbf{\Sigma}^{-\frac{1}{2}} = \mathbf{U}\mathbf{\Lambda}^{-\frac{1}{2}}\mathbf{U}^T$  is defined as ZCA transformation (also called Mahalanobis transformation, Kessy et al., 2018). The covariance matrix  $\mathbf{\Sigma} = 1/n\mathbf{F}^*\mathbf{F}^{*\text{T}}$  have orthonormal eigenvectors in columns of  $\mathbf{U}$  and eigenvalues on the diagonal of  $\mathbf{\Lambda}$ , so that  $\mathbf{\Sigma} = \mathbf{U}\mathbf{\Lambda}\mathbf{U}^T$ . Here the correlation coefficient between the rows of  $\mathbf{Z}^*$  is 0, but  $\mathbf{Z}^*$  is as close as possible to the original data  $\mathbf{F}^*$ . For more derivations and properties about ZCA transformation please see the paper of Kessy et al. (2018). Finally,  $\mathbf{Z}^*$  is transformed back to the original physical magnitude to obtain the decorrelated forcing variables  $\mathbf{Z}$ , where each row  $Z_i = Z_i^*\sigma_i + \bar{F}_i$ . Based on the decorrelated forcing data, we ran the experiment EXP-Z similar to CTRL-1D.

Replacing the  $\mathbf{F}$  in Equation 6 with the decorrelated forcing variables  $\mathbf{Z}$ , we get

$$\left(\frac{d\text{LSWT}}{dt}\right)_Z \approx \sum_i S_{ai} \frac{dZ_i}{dt} \quad (8)$$

where  $S_{ai}dZ_i/dt$  could be understood as the individual contribution from the  $i$ th forcing variable. Note that  $(d\text{LSWT}/dt)_Z$  does not contain the contribution of interactions among different atmospheric forcings that are contained in  $(d\text{LSWT}/dt)_F$  of Equation 6. So this contribution of interactions among different forcing variables could be represented as the difference of Equations 6 and 8, that is,  $(d\text{LSWT}/dt)_F - (d\text{LSWT}/dt)_Z \approx \sum_i S_{ai}dF_i/dt - \sum_i S_{ai}dZ_i/dt$ .

### 2.5. Linear Trend Analysis

The ordinary linear regression against time was used to estimate the long-term trend of variables and thereafter denoted by  $B \pm 2SE$ , where  $B$  and  $SE$  are estimated values of regression slope and standard error, with  $\pm 2SE$  as an approximation to the 95% confidence interval.

For two regressions with results of  $B_1 \pm 2SE_1$  and  $B_2 \pm 2SE_2$ , where their predictors are from the same population, Z-test was used to test whether the two slopes are equal significantly under the null hypothesis of  $B_1 - B_2 = 0$  (Clogg et al., 1995):

$$Z = \frac{B_1 - B_2}{\sqrt{(SE_1)^2 + (SE_2)^2}} \quad (9)$$

which was used to test whether there was a significant difference in the LSWT trends between EXP-F and CTRL-1D.

For those variables with a noticeable trend shift, piecewise linear regression (PLR) is an effective and intuitional way to detect the breakpoint (Ying et al., 2015). Here we assume that there is only one unknown endpoint located in an interval and no continuity constraint at the breakpoint. The significance of the PLR model could be tested by  $F$ -test and for more details refer to Toms and Lesperance (2003) and Ying et al. (2015).

## 3. Results

### 3.1. Model Validation

The simulation results from the experiment CTRL-2D during 2001–2018 are compared with MODIS in Figure 3a. As the remote-sensed satellite data are rather sparse during the ice-covered period (January–April) due to the wrong discrimination of clouds from lake ice or snow (Lazhu et al., 2016), we only carried out comparisons during the ice-free period (May–December). The model results showed a reasonable seasonal variation (Figure 3a) with a temporal correlation coefficient of 0.93. While there was still an overestimation of LSWT with mean bias and RMSE of 0.38°C and 1.47°C, respectively. This could be attributed to the skin effect and additional cold bias prevalent in MODIS data (Crosman & Horel, 2009; Wilson et al., 2013; Zhao et al., 2020).

Figures 3b and 3c present a comparison of observations and simulations of the thermal structure at the monitoring site in LNC during 2012–2013. The model well reproduced the characteristic of a dimictic lake that two thorough



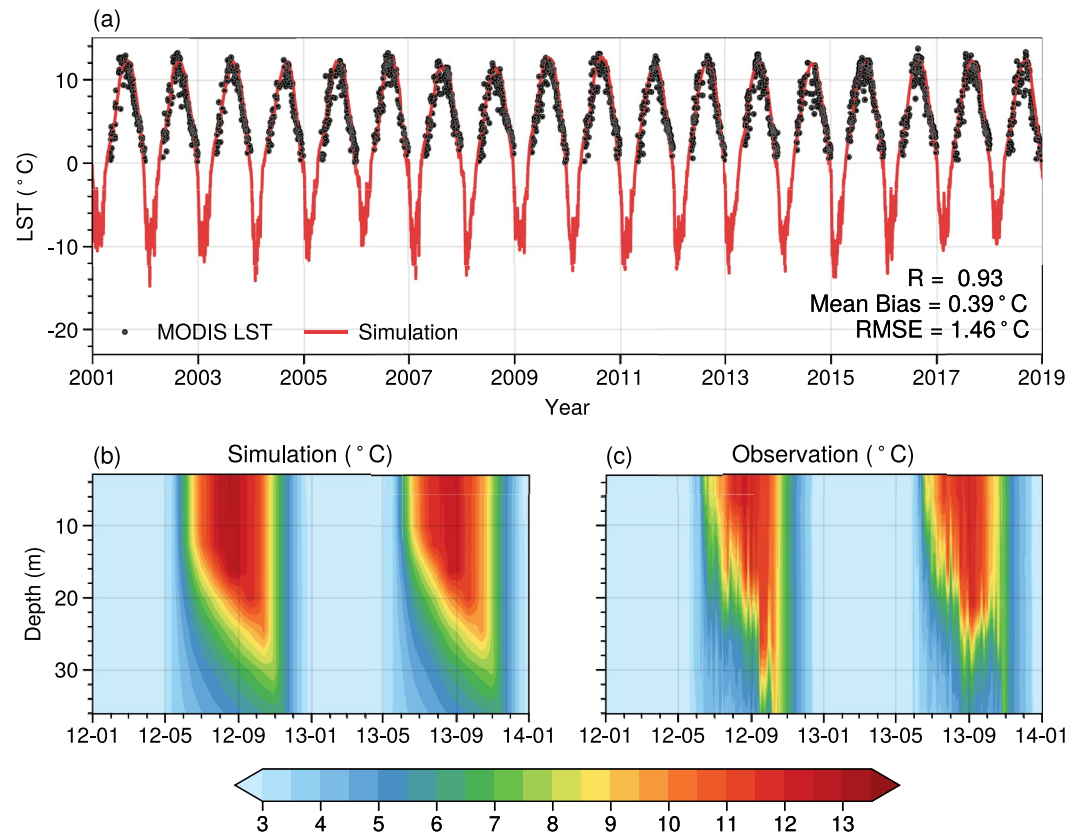


**Figure 3.** (a) The daily simulated land surface temperature (LST) (red solid line) and Moderate Resolution Imaging Spectroradiometer data (MODIS LST, black dots) during 2001–2018. The evolution of water temperature profile from simulations (b) and observations (c) during 2012–2013.

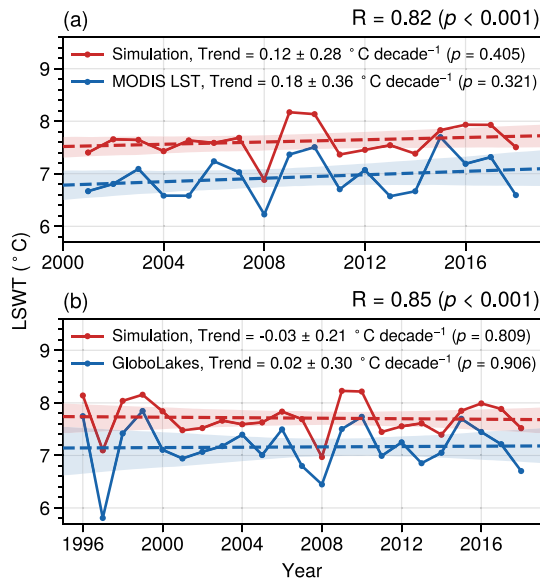
vertical mixing with a small temperature gradient occur before and after the summer thermal stratification (July–October), and the stratification is strongest in October with a metalimnion up to 30 m (Wang, Huang, et al., 2020).

The interannual variations of simulated LSWT basically accorded with MODIS data (Figure 4a) with a correlation coefficient  $R = 0.85$ , but with a smaller trend ( $0.12 \pm 0.28^\circ\text{C decade}^{-1}$ ) relative to MODIS data ( $0.18 \pm 0.36^\circ\text{C decade}^{-1}$ ) during the ice-free period, and the warming was not significant despite positive values. Spatially, as shown in Figures 5a and 5b, the simulations presented a similar pattern to MODIS over the central-eastern lake with the spatial correlation coefficient of 0.52 and the proportion of the grid points with the same sign (i.e., trends were in the same direction) is 74%. The simulation results were more spatially heterogeneous than MODIS and even cooled in the west, leading to the smaller spatially averaged trend than MODIS (Figure 4a). Extending the time to 1996 as with GloboLakes, there was still good consistency in the interannual variation ( $R = 0.82$ ) but a little trend in either simulation and GloboLakes (Figure 4b), and intralake heterogeneity increased with more cooling grid points (Figures 5c and 5d).

To sum up, the WRF-Lake model can well reproduce the seasonal evolution of LSWT and water temperature profile, as well as interannual variation and long-term trend over the last 20 years despite a warm systematic bias of approximately  $0.4^\circ\text{C}$ .

### 3.2. Lake Warming and Warming Hiatus

Different from the validation above, we only analyzed the trend from June to November (ice-free period common to all years 1980–2018) hereafter, because there was an apparent reduction of ice cover duration, that is, later freezing date in December and earlier break-up date in May from model results (not shown), which would overestimate the LSWT trend.



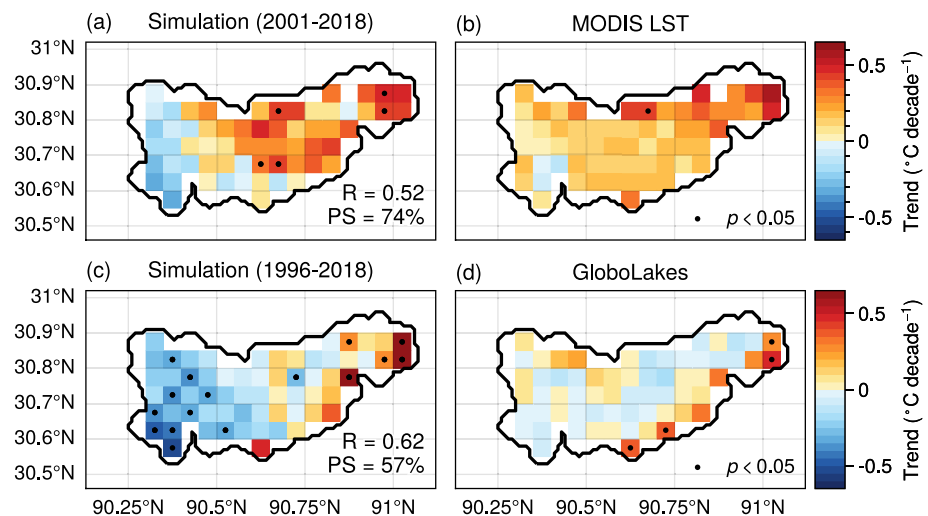
**Figure 4.** Interannual variation and long-term trend of simulated lake surface water temperature (red) compared with (a) Moderate Resolution Imaging Spectroradiometer data (MODIS LST, blue) during the ice-free period over 2001–2018 and with (b) GloboLakes (blue) over 1996–2018. Shaded areas indicate the confidence interval for the regression estimate.  $R$  is the interannual correlation coefficient. Note that the simulated values in each panel are retrieved only for the times corresponding to the satellite data, so the simulated values in the two panels are not identical.

Figure 6a shows the daily trends of simulated LSWT for the ice-free period with a significant shift around 1997 ( $p < 0.01$ ). The trends of LSWT at the days of a year during 1980–1997 were similar to those during 1980–2018, while there was almost no significant trend after 1997. In summer (July–September), the trend of  $0.23 \pm 0.10^\circ\text{C decade}^{-1}$  was smaller than in spring and autumn ( $0.35 \pm 0.10^\circ\text{C decade}^{-1}$ ) during 1980–2018.

Focusing on the average trend over the ice-free period (Figure 6b), the LSWT showed an overall upward trend of  $0.29 \pm 0.09^\circ\text{C decade}^{-1}$  over the past 40 years. The primary warming was completed before 1997 with an average trend of  $0.30 \pm 0.18^\circ\text{C decade}^{-1}$ , followed by a hiatus that the LSWT jumped by over  $1^\circ\text{C}$  after 1997. During this hiatus, the LSWT maintained an oscillation at over  $9^\circ\text{C}$  with a slightly negative trend of  $-0.08 \pm 0.24^\circ\text{C decade}^{-1}$  and a larger interannual variability (average of  $0.31^\circ\text{C yr}^{-1}$ ) than the warming stage ( $0.17^\circ\text{C yr}^{-1}$ ). The dramatic jump in LSWT in 1997/1998 directly resulted from the abrupt change in SAT (Figure 7a), which might be linked with the transition of the Atlantic Multidecadal Oscillation (AMO) from negative to positive phase (Feng & Hu, 2008; Zhang et al., 2020), and with strong El Niño event that raised the water level of TP lakes in that year (Hwang et al., 2016).

The timing of this hiatus after 1997 is fairly consistent with the previous report on a global scale that most lakes exhibited a warming hiatus to respond to the global warming hiatus during 1998–2009, where the SAT was the primary predictor and  $\text{SW}_l$  was secondary (Winslow et al., 2018; Zhong et al., 2016). However, as shown in Table 2 and Figure 7, the forcing variable SAT did not present a corresponding trend shifted to hiatus and even accelerated warming after 1997 due to the cloud-radiation feedback (Duan & Xiao, 2015). Owing to increasing moisture and deep cloud covers during

1980–2018 (Yang et al., 2012), the  $\text{SW}_l$  presented an overall declining trend, and it is notable that this declining trend weakened from  $-4.02 \pm 5.55$  to  $-0.24 \pm 6.69 \text{ W m}^{-2} \text{ decade}^{-1}$  since 1998. Hence the SAT and  $\text{SW}_l$  could not account for this hiatus with the global coincidence.



**Figure 5.** Spatial distributions of the lake surface water temperature trends in the simulations (a, c), Moderate Resolution Imaging Spectroradiometer retrievals over 2001–2018 (b), and GloboLakes over 1996–2018 (d). The black dots represent the significance at the  $p < 0.05$  level of T-test.  $R$  is the spatial correlation coefficient and PS is the proportion of the grid points with the same sign.

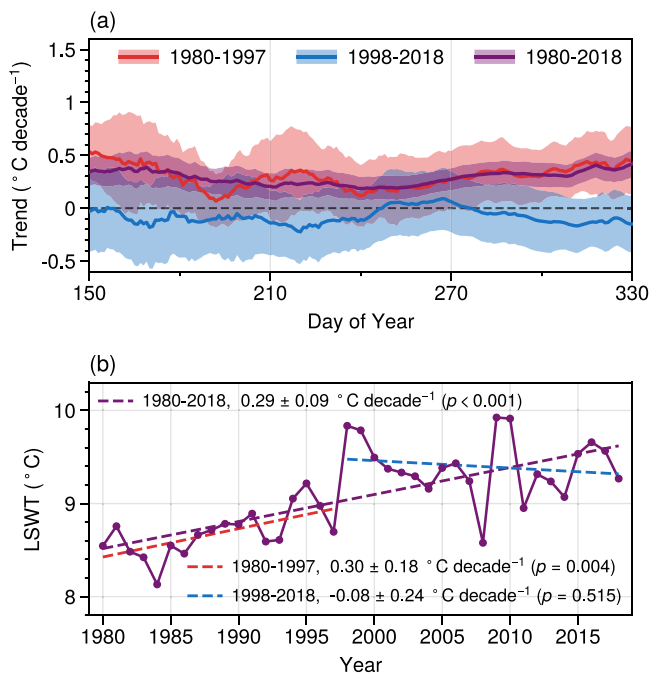


**Figure 6.** (a) Trends of simulated lake surface water temperature (LSWT) (solid lines) at the day of a year across different time spans during the ice-free period with the 95% confidence interval (shaded areas); (b) interannual variation (solid line) and trends (dashed lines) of simulated LSWT during 1980–1997 (red), 1998–2018 (blue), and 1980–2018 (purple).

Whereas the SSH and WS did show significant differences before and after 1997 (Table 2). Particularly the SSH turned from increasing to decreasing with an overall trend of  $0.08 \pm 0.23 \text{ g kg}^{-1} \text{ decade}^{-1}$ , and the increased SSH can raise LSWT by reducing the upward latent heat flux. The WS continued to decrease until the late 1990s and then shifted to a slightly increasing trend with an overall trend of  $-0.17 \pm 0.07 \text{ m s}^{-1} \text{ decade}^{-1}$  for 1980–2018, and the reduced WS could warm lakes by weakening the vertical mixing and surface turbulent heat fluxes in the lake, which have been widely observed in northern hemisphere lakes (Huang et al., 2012; Woolway et al., 2019).

As for the  $LW_{\downarrow}$ , it has an almost exact opposite trend to  $SW_{\downarrow}$  (Table 2) with a correlation coefficient of  $-0.71$  ( $p < 0.01$ ) between them, and there was almost no trend in their sum (total downward radiation,  $TR_{\downarrow}$ ). It could be assumed that the effects of long-term changes in  $LW_{\downarrow}$  and  $SW_{\downarrow}$  could counterbalance each other here if the response of the lake to them is equivalent on a long-term scale. Therefore, interdecadal changes in the SSH and WS might better explain the hiatus of lake warming after 1997.

The shifts of trends in LSWT and forcing variables above are accordingly reflected in the spatial distribution, as shown in Figure 8, where the surface pressure is omitted here because of its minimal trend relative to the other variables. LSWT changed faster in shallow areas than in deep areas (Figures 8a–8c) because the shallow water has a smaller heat capacity and is therefore more responsive to the changes in the overlying atmosphere. However, the shallow areas were not warmed or cooled uniformly; for example, the western shoal water of LNC warmed faster than the eastern water during 1980–1997 but cooled during 1998–2018 whereas the eastern water kept warming partially, which resulted in more pronounced warming in the east than west over 1980–2018. The differences should be attributed to the east-west heterogeneity of forcing variables' trends and their interdecadal shifts.

Before 1997, all variables showed relatively uniform distributions of trends, where all variables facilitated the rising LSWT excluding  $SW_{\downarrow}$ . During 1998–2018, the surface air warming was enhanced over eastern LNC based on pre-1997, and the SSH presented a decline in exact contrast to pre-1997; the WS showed a pattern of increasing (decreasing) trends over the western (eastern) LNC, and this east-west opposite mode can be neutralized by spatial averaging (Table 2) but still implied a link to the trend shift of LSWT. The spatial pattern of  $LW_{\downarrow}$  was the almost exact opposite of the  $SW_{\downarrow}$  during the three periods, hence there was almost no trend in the total downward radiation (Figures 8s–8u).

In summary, LNC was warmed before 1997 and then oscillated at a high level, that is, a warming hiatus. The decrease of SSH and recovered WS during the hiatus might be essential factors in counteracting the effects of the accelerated rising SAT over the period. Whereas the  $LW_{\downarrow}$  and  $SW_{\downarrow}$  almost counteracted each other during the entire 1980–2018.

### 3.3. Sensitivity of LSWT Response to Atmospheric Forcing Variables

Before discussing the quantitative contribution of each atmospheric forcing variable, we estimated the sensitivity of LSWT response to changes of forcing variables over the climatic mean state, based on the results of experiments EXP-F.

Within the range of historical climate extremes during 1980–2018, the multi-year average of LSWT varied quasi-linearly with the deviation of atmospheric forcing variables from the climatic mean state (red lines in Figure 9), and the slope was defined as the absolute sensitivity  $S_a$  that is validated as a constant here. The increasing thermodynamic variables, such as SAT, SSH,  $SW_{\downarrow}$ , and  $LW_{\downarrow}$ , would increase LSWT; increasing dynamical variables like WS would decrease LSWT on the contrary, whereas the slight perturbation of surface pressure

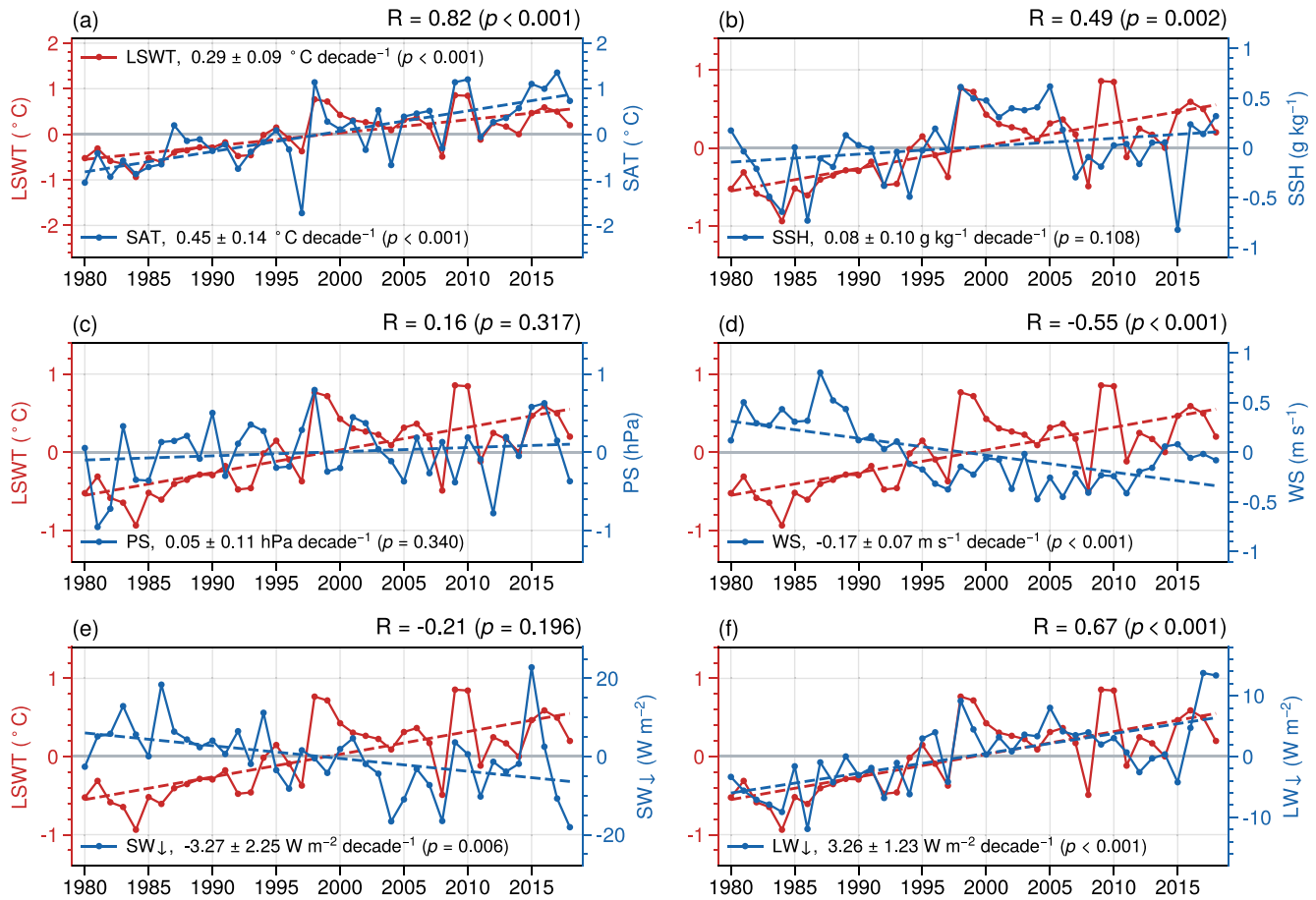


**Figure 7.** Interannual variations (solid lines) and trends (dashed lines) of the anomaly for lake surface water temperature (LSWT) (red) and forcing variables (blue): (a) surface air temperature (SAT), (b) surface specific humidity (SSH), (c) surface pressure (SP), (d) 10 m wind speed (WS), (e) downward shortwave radiation ( $SW_{\downarrow}$ ), and (f) downward longwave radiation ( $LW_{\downarrow}$ ).  $R$  is the correlation coefficient between LSWT and each forcing variable with the corresponding  $p$ -value.

produced no significant impact on LSWT. Note that  $SW_{\downarrow}$  and  $LW_{\downarrow}$  equally affect LSWT numerically with  $S_a$  of  $0.043^{\circ}\text{C} (\text{W m}^{-2})^{-1}$  and  $0.040^{\circ}\text{C} (\text{W m}^{-2})^{-1}$ , which confirms our previous assumption that the response of the LSWT to them is equal on a long-term scale.

**Table 2**

*The Trends Across Different Time Spans of LSWT and Forcing Variables, With the Significance Level of Differences in Trends Before and After 1997*

Variables	Trend			$p$ -value
	1980–1997	1998–2018	1980–2018	
LSWT ( $^{\circ}\text{C decade}^{-1}$ )	$0.30 \pm 0.18$	$-0.08 \pm 0.24$	$0.29 \pm 0.09$	0.001
SAT ( $^{\circ}\text{C decade}^{-1}$ )	$0.13 \pm 0.43$	$0.38 \pm 0.37$	$0.45 \pm 0.14$	0.415
SSH ( $\text{g kg}^{-1} \text{decade}^{-1}$ )	$0.10 \pm 0.25$	$-0.31 \pm 0.21$	$0.08 \pm 0.23$	0.013
SP ( $\text{hPa decade}^{-1}$ )	$0.31 \pm 0.33$	$-0.06 \pm 0.29$	$0.05 \pm 0.11$	0.096
WS ( $\text{m s}^{-1} \text{decade}^{-1}$ )	$-0.40 \pm 0.21$	$0.09 \pm 0.12$	$-0.17 \pm 0.07$	<0.001
$SW_{\downarrow}$ ( $\text{W m}^{-2} \text{decade}^{-1}$ )	$-4.02 \pm 5.55$	$-0.24 \pm 6.69$	$-3.27 \pm 2.25$	0.384
$LW_{\downarrow}$ ( $\text{W m}^{-2} \text{decade}^{-1}$ )	$3.76 \pm 3.35$	$0.48 \pm 3.32$	$3.26 \pm 1.23$	0.164
$TR_{\downarrow}$ ( $\text{W m}^{-2} \text{decade}^{-1}$ )	$0.16 \pm 1.65$	$-0.38 \pm 3.59$	$0.30 \pm 5.32$	0.998

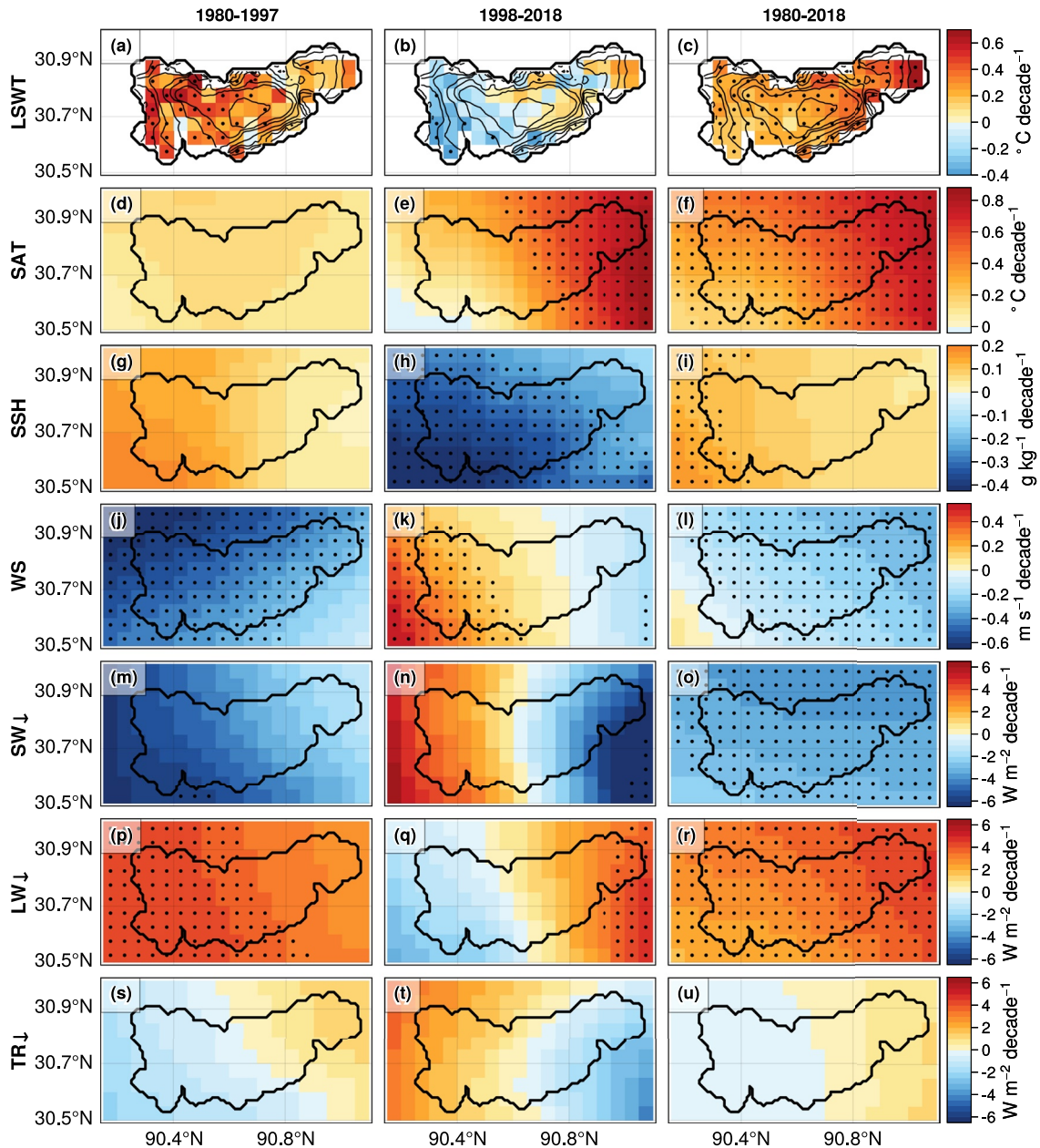


**Figure 8.** The trend (shaded area) of the anomaly for (a–c) lake surface water temperature (LSWT) and atmospheric forcing variables (d–f) surface air temperature (SAT), (g–i) surface specific humidity (SSH), (j–l) 10 m wind speed (WS), (m–o) downward shortwave radiation ( $SW_{\downarrow}$ ), (p–r) downward longwave radiation ( $LW_{\downarrow}$ ), and (s–u) total downward radiation ( $TR_{\downarrow}$ ) during 1980–1997 (column 1), 1998–2018 (column 2), and 1980–2018 (column 3). The contours in (a–c) indicate the bathymetry, and the black dots represent the significance at the  $p < 0.05$  level. The labels of colorbars are units of the long-term trends of variables.

Relative sensitivity  $S_r$  was defined for comparability across all forcing variables (see subsection 2.4.1). The results show that the most influential factor on LSWT is  $SW_{\downarrow}$  with  $S_r = 0.59^{\circ}\text{C}$ , followed by a comparable extent of SAT ( $0.39^{\circ}\text{C}$ ),  $LW_{\downarrow}$  ( $0.37^{\circ}\text{C}$ ), WS ( $-0.36^{\circ}\text{C}$ ), and finally by the SSH ( $0.30^{\circ}\text{C}$ ). The strong effects of radiation and temperature are as expected because they are characteristics of high-altitude lakes (Kirillin et al., 2017; Wen et al., 2016), whereas the SSH and WS show a greater impact on LSWT change in LNC relative to Ngoring Lake that is a large but shallow freshwater lake on TP with elevation also over 4,000 m (Wen et al., 2016).

Contrasting with the symmetric responses of LSWT to the opposite anomalous climates (red lines in Figure 9), the responses of long-term LSWT trend are asymmetrical (blue lines in Figure 9) for changing thermodynamic variables. Specifically, the long-term warming trends of the lake tend to be amplified in the climates that induced

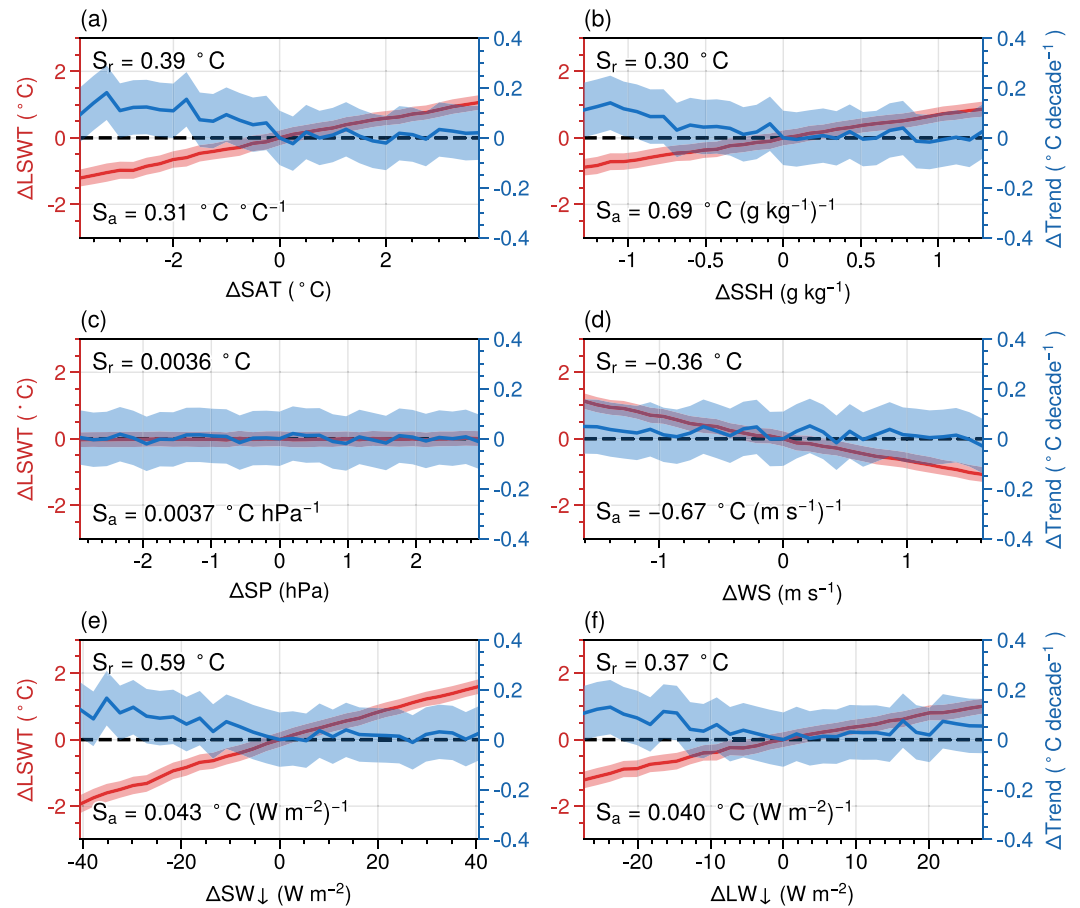


**Figure 9.** Changes in multi-year average (red lines) and long-term trend (blue lines) of LSWT with perturbed atmospheric forcing variables: (a) surface air temperature (SAT), (b) surface specific humidity (SSH), (c) surface pressure (SP), (d) 10 m wind speed (WS), (e) downward shortwave radiation ( $SW_{\downarrow}$ ), and (f) downward longwave radiation ( $LW_{\downarrow}$ ), including the values of absolute sensitivity ( $S_a$ ) and relative sensitivity ( $S_r$ ). Shaded areas indicate the 95% confidence intervals. All changes ( $\Delta$ ) are the differences between the simulation of each sensitive experiment and the control experiment simulation. The other forcing variables are kept in their original values for each group of individual experiments.

lower climatic mean LSWT (Cold Climate, CC) but little change in the opposite climates (Warm Climate, WC). Because during the warming stage (e.g., 1980–1997 as shown in Figure 10a), the cooling in CC relative to the normal climate (NC) is more pronounced than the warming in NC, and thereafter the two deviations relative to NC are of comparable magnitude; thus the warming trend appears to be amplified in CC. But the situation is not present in the experiments on WS (Figure 10b). These phenomena might be explained qualitatively by the impact of atmospheric forcing variables on the timing of thermal stratification.

The LSWT during an ice-free period is greatly governed by the timing of thermal stratification when the LSWT is above  $Td_{max}$ , because the lake is mixing up and down before then with a limited rate of rise in LSWT (Boehrer & Schultze, 2008). In the extreme CC, both the timings of ice-off and thermal stratification are delayed by approximately 15 days around May (Figure 10c) and the increased albedo causes a decrement of absorbed solar radiation in May relative to NC, leading to a lower base temperature in June. In WC, the increment of absorbed solar radiation in April is insufficient to match the reduction in May in CC owing to the solar radiation peaking in May before the rainy season (You et al., 2007). Hence, the number of days advanced for the onset of thermal stratification in WC is less than the delay in CC (Figure 10e), which may explain why the daily LSWT in WC is closer to NC (Figure 10c).

But likewise in WC, the decrease of WS attenuates not only the surface heat flux but also the vertical mixing (Huang et al., 2012; Woolway et al., 2019), which directly weakens the mixing after ice melt and brings earlier

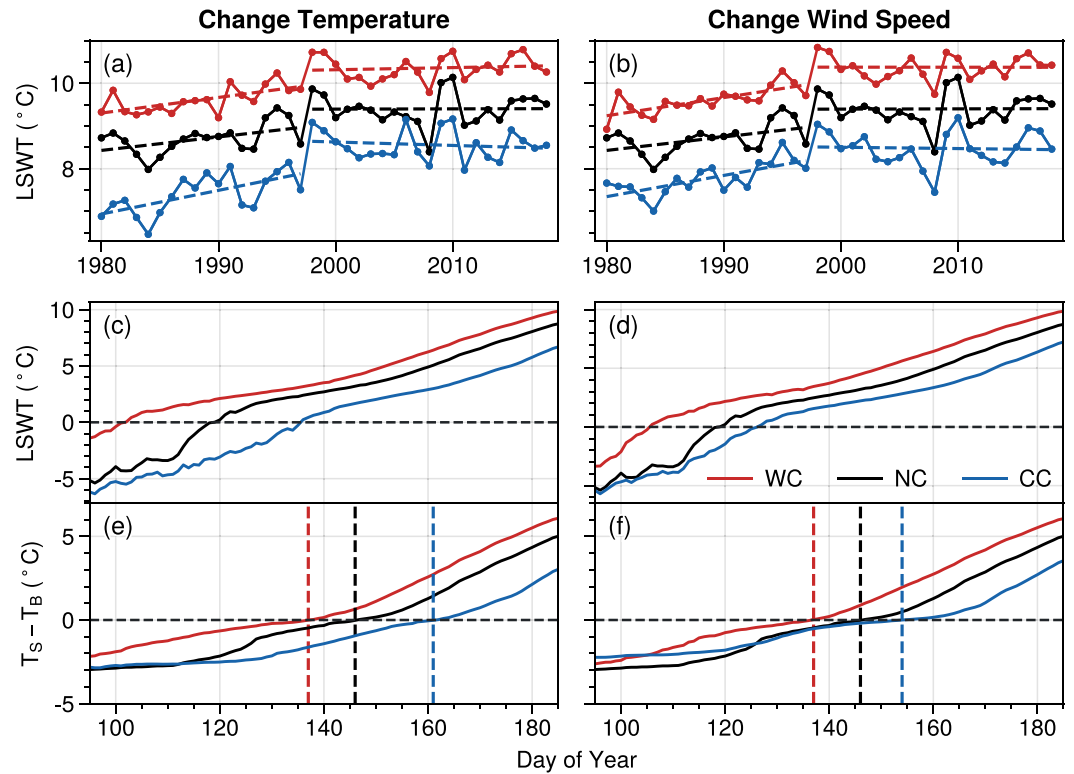


**Figure 10.** (a–b) Interannual variations (solid lines) and trends (before and after 1997; dashed lines) of LSWT in warm climate (WC, red lines), normal climate (NC, black lines), and cold climate (CC, blue lines); (c–d) daily lake surface water temperature (LSWT) and (e–f) daily temperature difference between subsurface ( $T_s$ , at 0.5 m) and bottom ( $T_b$ , at 50 m), averaged during 1980–1997. LSWT = 0°C was considered as the timing of ice-off in (c–d);  $T_s - T_b > 0^\circ\text{C}$  was considered as the onset of thermal stratification, which is indicated by vertical dashed lines in (e–f). The left and right columns illustrate the effects of changes in surface air temperature and 10 m wind speed, respectively.

thermal stratification and thereby raises the later base LSWT in NC (Figures 10d and 10f). Thus, the response of the LSWT trend to the WS is symmetrical relative to the thermodynamical variables.

The phenomena described above suggest that the changes in meteorological forcing variables before May can influence LSWT after June by adjusting the timing of ice-off and thermal stratification (Austin & Colman, 2007). This delayed effect is more pronounced in colder and deeper lakes due to the larger heat capacity (Woolway & Merchant, 2017).

### 3.4. Contributions of Atmospheric Forcing Variables to the Trend of LSWT

Here we need to validate the second assumption in Equation 6 that is,  $\partial LSWT / \partial F \approx S_a$ . To this end, we estimated the interannual variation by the forward Euler difference based on Equation 6 using simulated annual mean LSWT in 1980 as the initial value, and the estimated interannual increments should be close to the simulation if the assumption is acceptable. As shown in Figures 11a and 11b, the estimation results reproduce the rising and hiatus of LSWT with a correlation coefficient of up to 0.93 with the simulation results, and the interannual increments (calculated by backward difference) of the estimated and simulated results are close with a correlation coefficient of 0.82. The estimated long-term trend is overestimated but still acceptable.

Considering the effects of interactions among forcing variables on the long-term LSWT trend, we compared the simulations of CTRL-1D and EXP-Z driven by the original and decorrelated forcing data in Figure 11c, respectively. EXP-Z produces a smaller trend ( $0.21 \pm 0.09^\circ\text{C decade}^{-1}$ ) than CTRL-1D ( $0.29 \pm 0.09^\circ\text{C decade}^{-1}$ ), and the reduction of  $0.08^\circ\text{C decade}^{-1}$  (accounting for 27.6% of CTRL-1D) is interpreted as the cross contribution of interactions among forcing variables, which is indeed important to the long-term LSWT trend of LNC.

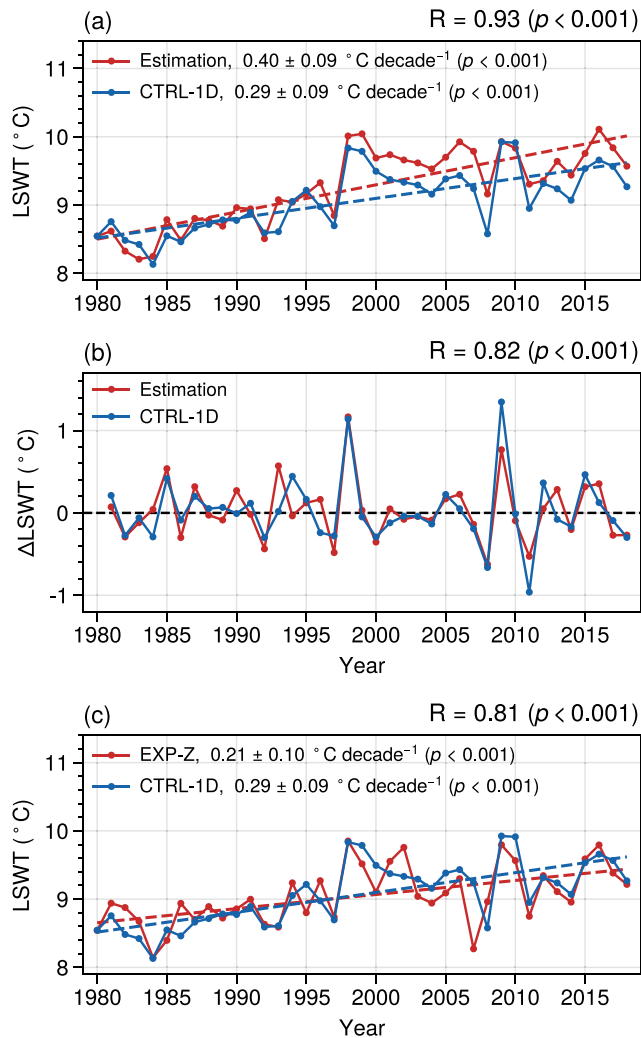


**Figure 11.** (a) Estimated (red) and simulated (blue) interannual variations (solid lines) of lake surface water temperature with long-term trends (dashed lines) based on original forcing data, and their (b) interannual increments. (c) Comparison between simulations based on original (blue) and decorrelated (red) forcing data.  $R$  is the correlation coefficient between two series with the corresponding  $p$ -value.

Based on Equations 6 and 8, we further estimated the individual contributions and cross contribution of atmospheric forcing variables to the trend of LSWT. During 1980–2018 (Figure 12a), the weakened WS, rising SAT, and increased  $LW_1$  caused the main LNC warming with contributions of 0.14, 0.12, and  $0.08^\circ\text{C decade}^{-1}$ , respectively. The contribution rates of WS, SAT, and  $LW_1$  to the estimated long-term LSWT trend ( $0.4^\circ\text{C decade}^{-1}$ ) were about 35%, 30%, and 20%. The decline of  $SW_1$  caused a negative contribution of  $-0.06^\circ\text{C decade}^{-1}$  (–15%); the SSH contributed only  $-0.01^\circ\text{C decade}^{-1}$  (–2.5%) because of its more flatter and even negative trend on the long-term scale after decorrelating; the surface air pressure contributing 0.08% of LSWT trend is omitted here for its negligible effect. The cross contribution from the interactions among forcing variables contributed  $0.13^\circ\text{C decade}^{-1}$  (32.5%), which is close to the contribution rate of 27.6% derived from CTRL-1D and EXP-Z.

As shown in Figure 12b, the contributions of independently varying (decorrelated) forcing variables also retained interdecadal shifts before and after 1997, but there was no significant shift in the contribution of  $SW$  and cross contribution among different forcing variables. The primary lake warming before 1997 was contributed by the weakened WS and increased  $LW_1$ , which led to the LSWT warmed by  $0.22$  and  $0.18^\circ\text{C decade}^{-1}$ , respectively. However, they showed much smaller contributions of  $0.05^\circ\text{C decade}^{-1}$  to the LSWT trend after 1997, which slowed down the LNC warming. The individual contribution of SAT was mainly shown after 1997 ( $0.11^\circ\text{C decade}^{-1}$ ). The SSH showed a remarkable negative contribution of  $-0.25^\circ\text{C decade}^{-1}$  to the LSWT trend after 1997 despite little impact before 1997. Thus SSH played a non-negligible role in the shift from warming to cooling trend of LNC before and after 1997, which was overlooked in previous studies.

## 4. Discussion

### 4.1. Comparison With Previous Studies

In this study, LNC was warmed slower than the ambient air during ice-free period, which is opposite to a global-scale survey revealing that ice-covered lakes are typically warming faster than ambient air (O'Reilly et al., 2015). In fact, the rapid warming of many ice-covered lakes are associated with increases in both summer SAT and  $SW_1$  (O'Reilly et al., 2015), and ice cover reduction plays a minor role (Zhong et al., 2016). But in LNC, the  $SW_1$  as a source of energy declined significantly with a trend of  $-3.27 \pm 2.25 \text{ W m}^{-2}$  (Figure 7e), and this decline was also prevalent in other areas of TP (Yang

et al., 2012), for example, which could even offset the lake warming from SAT in Lake Ngoring and Lake Gyaring (Kirillin et al., 2017). In this view, we consider that the decline of  $SW_1$  is an important reason why the warming of LNC is different from that of other ice-covered lakes worldwide.

Another study on LNC showed a lake warming rate in summer (July–September) of  $0.52 \pm 0.25^\circ\text{C decade}^{-1}$  during 1979–2012 (Huang et al., 2017), which is close to but less than the air warming rate in their study and greatly more than our result of  $0.28 \pm 0.14^\circ\text{C decade}^{-1}$  during the same period. The huge difference could be partly explained. First, their daily average simulation result is lower than the observation (Figure 6 in Huang et al., 2017) and we assume it is a systematic bias. Then the simulated lake system is actually in a cold state relative to the real state and therefore the warming rate tends to be amplified based on the analyses in Section 3.3 (Figure 10).

In addition to the contributions to LNC warming from SAT and  $LW_1$  (Huang et al., 2017; Su et al., 2019), this study emphasized the role of interdecadal shifts in SSH on the LNC warming hiatus after 1997. Further, we



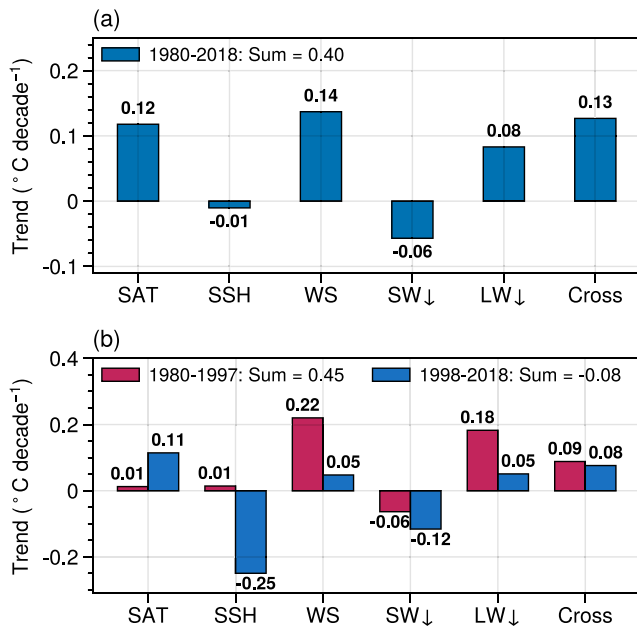


**Figure 12.** (a) Estimated individual contribution of surface air temperature (SAT), surface specific humidity (SSH), and 10 m wind speed (WS), surface downward shortwave radiation (SW<sub>↓</sub>), surface downward longwave radiation (LW<sub>↓</sub>), and their cross contribution (Cross) to the long-term trend of LSWT during 1980–2018; (b) Estimated contributions during 1980–1997 (red) and 1998–2018 (blue). The Sum in legends represents the summation of all bars.

quantitatively estimated the individual contributions of each forcing variable and the cross contribution of their interactions to the LSWT long-term trend of LNC during 1980–2018.

#### 4.2. About the Attribution Method

In Equation 6, we simply linearized the lake system on an interannual scale and assumed the absolute sensitivity (partial derivative)  $S_{a_i}$  is a constant. But it is natural that the  $S_{a_i}$  of a given forcing variable  $F_i$  should depend on the state of other variables  $F_j$ , that is,  $S_{a_i}(t) = S_{a_i}(F_j(t))$ . We calculated the time-varying  $S_{a_i}(t)$  in every year to represent the variation of atmospheric states, then repeated the calculations similar to Figures 11a and 11b. However, there was no significant improvement in the estimated long-term trend and interannual increments (not shown). So the overestimated LSWT trend (Figure 11a) could not be attributed to the assumption of constant  $S_{a_i}$ , and we speculated this error might be related to the neglected high-order partial derivative (Chen et al., 2020) because some variables showed significant interdecadal shifts. Anyway, our results still provide a quantitative perspective for understanding the relative contribution of different atmospheric forcing variables to the long-term trend of LSWT in LNC.

#### 4.3. Other Deficiencies

There are still some deficiencies to be improved in this study. In the 1-D lake model WRF-Lake, the heat fluxes from inflows and outflows are unresolved but important for glacial-fed lakes such as LNC (Fink et al., 2014; Wan et al., 2018). Additionally, some key parameters such as the light extinction coefficient should provide feedback on the state of lakes through biochemical

processes but it was set to a constant, which may underestimate the impact of climate changes on the lake system (Rose et al., 2016). Moreover, the 1-D lake model ignores horizontal exchanges of momentum and energy, which are important processes for heat transfer and can be further resolved by 3-D models (Wu et al., 2021).

Besides, this study was based on offline simulations with the given external forcing conditions that were not obtained from the lake surface, whereas the lake surface is coupled with the overlying atmosphere in real-time and thus some feedback processes are ignored. For instance, a weakening of the lake-air temperature gradient induces a more stable boundary layer and thereby smaller wind speed by altering local circulation (Desai et al., 2009). But this error should not be major because the interannual anomalies of the forcing variables are dominated by the larger-scale circulation, which tends to be regionally consistent (Huang et al., 2012; Livingstone & Padišák, 2007).

### 5. Summary

In this study, the 1-D lake model WRF-Lake was driven by the corrected CMFD to simulate the daily LSWT in LNC on TP during 1980–2018. The model could well reproduce the seasonal variation of LSWT and thermal structure with a warm bias of approximately 0.4°C in LSWT compared to the MODIS and in-situ observations. Furthermore, the simulation results also show that the interannual variation and long-term trends of LSWT are close to the MODIS data during 2001–2018.

The results show that LNC was warmed with a long-term trend of  $0.29 \pm 0.09^\circ\text{C decade}^{-1}$  during the ice-free period, which was smaller than the trend of local SAT ( $0.45 \pm 0.14^\circ\text{C decade}^{-1}$ ) during the past 40 years. The primary warming was completed before 1997 ( $0.30 \pm 0.18^\circ\text{C decade}^{-1}$ ) followed by a hiatus that the LSWT jumped to a relatively warmer state and maintained an oscillation with a slightly negative trend of  $-0.08 \pm 0.24^\circ\text{C decade}^{-1}$  after 1997.

The sensitivity of LSWT response to the atmospheric forcing variables was studied by a series of sensitivity experiments. Within the range of historical climate extremes, LSWT was most sensitive to the climatic perturbation

in  $SW_{\downarrow}$ , followed by a comparable extent of SAT,  $LW_{\downarrow}$ , WS, and finally the SSH. Moreover, the long-term lake warming trends tend to be amplified under a cold lake state induced by thermodynamical variables such as SAT.

We further estimated the individual contributions and cross contribution of atmospheric forcing variables to the long-term LSWT trend of LNC. The weakened WS, rising SAT, and increased  $LW_{\downarrow}$  were the most remarkable factors warming the LNC with the independent contribution rates of about 35%, 30%, and 20% to the long-term LSWT trend during 1980–2018, respectively. Whereas the decline of  $SW_{\downarrow}$  caused a negative contribution rate of –15%. The interaction of all atmospheric forcing variables shows a positive contribution rate of 32.5%. Particularly, despite the slight contribution of SSH (–2.5%) to the long-term LSWT trend of LNC, the interdecadal shift of SSH trend from increasing to decreasing (Table 2) around 1997 played a non-negligible role in the hiatus of LNC warming after 1997.

Overall, we quantitatively estimated the individual and cross contributions of different atmospheric factors to the long-term LSWT trend during 1980–2018. Meanwhile, we also showed the particularity of warming for a TP lake compared to other ice-covered lakes worldwide. Further work should conduct an integrated study of more lakes on TP based on the model or remote sensing information, for an overall understanding of climate change impacts on the TP lakes.

### Data Availability Statement

These datasets were used in this study: the China Meteorological Forcing Data set (He et al., 2020, available at <https://data.tpc.ac.cn/en/data/8028b944-daaa-4511-8769-965612652c49/>), the Moderate Resolution Imaging Spectroradiometer (MODIS/Terra) Version 6.1 MOD11A1 and MOD11A2 (Wan et al., 2015a; 2015b, available at [https://lpdaac.usgs.gov/product\\_search/?query=MOD11%26view=cards%26sort=title](https://lpdaac.usgs.gov/product_search/?query=MOD11%26view=cards%26sort=title)), the GloboLakes LSWT Data set (Carrea & Merchant, 2019, available at <https://doi.org/10.24381/cds.d36187ac>), the daily data from the weather station on the southeastern shore of Lake Nam Co during 2006–2018 (Wang & Wu, 2018, 2019, available at <http://poles.tpc.ac.cn/en/data/c97bce0f-bf67-4dcc-b864-d7e4d8cff62f/>), and the long-term data set of integrated land-atmosphere interaction observations on the Tibetan Plateau during 2005–2016 (Ma, 2020, available at <http://dx.doi.org/10.11888/Meteoro.tpc.270910>).

Software - Calculations in this study were made with the GNU Fortran compiler (GFortran) version 7.5.0 which are available under the terms of the GNU General Public License at <https://gcc.gnu.org/wiki/GFortran-Source>. All figures were made by the open-source Python package ProPlot (V0.7.0, available from <https://proplot.readthedocs.io/>).

### Acknowledgments

This study is supported by National Natural Science Foundation of China under Grants 41975081, 41975130, and the National Key R&D Program of China under Grant 2017YFA0604301, CAS “Light of West China” Program (E12903010, Y929641001), the Research Funds for the Frontiers Science Center for Critical Earth Material Cycling Nanjing University, the Fundamental Research Funds for the Central Universities (020914380103), the Jiangsu University “Blue Project” outstanding young teachers training object, and the Jiangsu Collaborative Innovation Center for Climate Change. The authors thank Dr. Junbo Wang and Dr. Lei Huang for providing us the observation data of Lake Nam Co. The authors show our deepest respect and appreciation to the two anonymous reviewers for their insightful and constructive suggestions to help us significantly improve the manuscript.

### References

- Adrian, R., O'Reilly, C. M., Zagarese, H., Baines, S. B., Hessen, D. O., Keller, W., et al. (2009). Lakes as sentinels of climate change. *Limnology and Oceanography*, 54(6), 2283–2297. [https://doi.org/10.4319/lo.2009.54.6\\_part\\_2.2283](https://doi.org/10.4319/lo.2009.54.6_part_2.2283)
- Anderson, E. J., Stow, C. A., Gronewold, A. D., Mason, L. A., McCormick, M. J., Qian, S. S., et al. (2021). Seasonal overturn and stratification changes drive deep-water warming in one of Earth's largest lakes. *Nature Communications*, 12(1), 1688. <https://doi.org/10.1038/s41467-021-21971-1>
- Anyah, R. O., & Semazzi, F. H. M. (2004). Simulation of the sensitivity of Lake Victoria basin climate to lake surface temperatures. *Theoretical and Applied Climatology*, 79(1), 55–69. <https://doi.org/10.1007/s00704-004-0057-4>
- Austin, J. A., & Colman, S. M. (2007). Lake superior summer water temperatures are increasing more rapidly than regional air temperatures: A positive ice-albedo feedback. *Geophysical Research Letters*, 34(6), L06604. <https://doi.org/10.1029/2006GL029021>
- Bocinsky, R. K., & Kohler, T. A. (2014). A 2,000-year reconstruction of the rain-fed maize agricultural niche in the US Southwest. *Nature Communications*, 5(1), 5618. <https://doi.org/10.1038/ncomms6618>
- Boehrer, B., & Schultze, M. (2008). Stratification of lakes. *Reviews of Geophysics*, 46(2), RG2005. <https://doi.org/10.1029/2006RG000210>
- Bolton, D. (1980). The computation of equivalent potential temperature. *Monthly Weather Review*, 108(7), 1046–1053. [https://doi.org/10.1175/1520-0493\(1980\)108<1046:TCOEPT>2.0.CO;2](https://doi.org/10.1175/1520-0493(1980)108<1046:TCOEPT>2.0.CO;2)
- Butcher, J. B., Nover, D., Johnson, T. E., & Clark, C. M. (2015). Sensitivity of lake thermal and mixing dynamics to climate change. *Climatic Change*, 129(1), 295–305. <https://doi.org/10.1007/s10584-015-1326-1>
- Carrea, L., & Merchant, C. J. (2019). GloboLakes: Lake surface water temperature (LSWT) v4.0 (1995–2016) (Version 3.1). Centre for Environmental Data Analysis (CEDA). <https://doi.org/10.5285/76A29C5B55204B66A40308FC2BA9CDB3>
- Chen, C., Wang, L., Myneni, R. B., & Li, D. (2020). Attribution of land-use/land-cover change induced surface temperature anomaly: How accurate is the first-order Taylor series expansion? *Journal of Geophysical Research: Biogeosciences*, 125(9), e2020JG005787. <https://doi.org/10.1029/2020JG005787>
- Clogg, C. C., Petkova, E., & Haritou, A. (1995). Statistical methods for comparing regression coefficients between models. *American Journal of Sociology*, 100(5), 1261–1293. <https://doi.org/10.1086/230638>

- Cohen, A. S., Gergurich, A. S., Kraemer, B. M., McGlue, M. M., McIntyre, P. B., Russell, J. M., et al. (2016). Climate warming reduces fish production and benthic habitat in Lake Tanganyika, one of the most biodiverse freshwater ecosystems. *Proceedings of the National Academy of Sciences*, *113*(34), 9563–9568. <https://doi.org/10.1073/pnas.1603237113>
- Crosman, E. T., & Horel, J. D. (2009). MODIS-derived surface temperature of the Great salt lake. *Remote Sensing of Environment*, *113*(1), 73–81. <https://doi.org/10.1016/j.rse.2008.08.013>
- Desai, A. R., Austin, J. A., Bennington, V., & McKinley, G. A. (2009). Stronger winds over a large lake in response to weakening air-to-lake temperature gradient. *Nature Geoscience*, *2*(12), 855–858. <https://doi.org/10.1038/ngeo693>
- Du, J., Wen, L., & Su, D. (2019). Reliability of three reanalysis datasets in simulation of three alpine lakes on the Qinghai-Tibetan plateau (in Chinese with english abstract). *Plateau Meteorology*, *38*(1), 101–113. <https://doi.org/10.7522/j.issn.1000-0534.2018.00110>
- Duan, A., & Xiao, Z. (2015). Does the climate warming hiatus exist over the Tibetan Plateau? *Scientific Reports*, *5*(1), 13711. <https://doi.org/10.1038/srep13711>
- Fang, N., Yang, K., LazhuChen, Y., Wang, J., & Zhu, L. (2017). Research on the application of WRF-lake modeling at Nam Co lake on the Qinghai-Tibetan plateau (in chinese with english abstract). *Plateau Meteorology*, *36*(3), 610–618. <https://doi.org/10.7522/j.issn.1000-0534.2016.00038>
- Feng, S., & Hu, Q. (2008). How the North Atlantic Multidecadal Oscillation may have influenced the Indian summer monsoon during the past two millennia. *Geophysical Research Letters*, *35*(1), L01707. <https://doi.org/10.1029/2007GL032484>
- Fink, G., Schmid, M., Wahl, B., Wolf, T., & Wüest, A. (2014). Heat flux modifications related to climate-induced warming of large European lakes. *Water Resources Research*, *50*(3), 2072–2085. <https://doi.org/10.1002/2013WR014448>
- Grant, L., Vanderkelen, I., Gudmundsson, L., Tan, Z., Perroud, M., Stepanenko, V. M., et al. (2021). Attribution of global lake systems change to anthropogenic forcing. *Nature Geoscience*, *14*(11), 849–854. <https://doi.org/10.1038/s41561-021-00833-x>
- Gu, H., Jin, J., Wu, Y., Ek, M. B., & Subin, Z. M. (2015). Calibration and validation of lake surface temperature simulations with the coupled WRF-lake model. *Climatic Change*, *129*(3), 471–483. <https://doi.org/10.1007/s10584-013-0978-y>
- Hafner, T. A., & Smith, R. B. (1985). Pressure drag on the European alps in relation to synoptic events. *Journal of the Atmospheric Sciences*, *42*(6), 562–575. [https://doi.org/10.1175/1520-0469\(1985\)042<0562:PDOTEA>2.0.CO;2](https://doi.org/10.1175/1520-0469(1985)042<0562:PDOTEA>2.0.CO;2)
- He, J., Yang, K., Tang, W., Lu, H., Qin, J., Chen, Y., & Li, X. (2020). The first high-resolution meteorological forcing dataset for land process studies over China. *Scientific Data*, *7*(1), 25. <https://doi.org/10.1038/s41597-020-0369-y>
- Henderson-Sellers, B. (1985). New formulation of eddy diffusion thermocline models. *Applied Mathematical Modelling*, *9*(6), 441–446. [https://doi.org/10.1016/0307-904X\(85\)90110-6](https://doi.org/10.1016/0307-904X(85)90110-6)
- Hostetler, S., & Bartlein, P. (1990). Simulation of lake evaporation with application to modeling lake level variations of Harney-Malheur Lake, Oregon. *Water Resources Research*, *20*(10), 2603–2612. <https://doi.org/10.1029/WR0261010P02603>
- Huang, A., Lazhu, Wang, J., Dai, Y., Yang, K., Wei, N., et al. (2019). Evaluating and improving the performance of three 1-d lake models in a large deep lake of the central Tibetan plateau. *Journal of Geophysical Research: Atmospheres*, *124*(6), 3143–3167. <https://doi.org/10.1029/2018JD029610>
- Huang, A., Rao, Y. R., & Zhang, W. (2012). On recent trends in atmospheric and limnological variables in lake Ontario. *Journal of Climate*, *25*(17), 5807–5816. <https://doi.org/10.1175/JCLI-D-11-00495.1>
- Huang, L., Wang, J., Zhu, L., Ju, J., & Daut, G. (2017). The warming of large lakes on the Tibetan plateau: Evidence from a lake model simulation of Nam Co, China, during 1979–2012. *Journal of Geophysical Research: Atmospheres*, *122*(24), 13095–13107. <https://doi.org/10.1002/2017JD027379>
- Hwang, C., Cheng, Y.-S., Han, J., Kao, R., Huang, C.-Y., Wei, S.-H., & Wang, H. (2016). Multi-decadal monitoring of lake level changes in the Qinghai-tibet plateau by the TOPEX/poseidon-family altimeters: Climate implication. *Remote Sensing*, *8*(6), 446. <https://doi.org/10.3390/rs8060446>
- Kessy, A., Lewin, A., & Strimmer, K. (2018). Optimal whitening and decorrelation. *The American Statistician*, *72*(4), 309–314. <https://doi.org/10.1080/00031305.2016.1277159>
- Kirillin, G., Wen, L., & Shatwell, T. (2017). Seasonal thermal regime and climatic trends in lakes of the Tibetan highlands. *Hydrology and Earth System Sciences*, *21*(4), 1895–1909. <https://doi.org/10.5194/hess-21-1895-2017>
- Kraemer, B. M., Anneville, O., Chandra, S., Dix, M., Kuusisto, E., Livingstone, D. M., et al. (2015). Morphometry and average temperature affect lake stratification responses to climate change. *Geophysical Research Letters*, *42*(12), 4981–4988. <https://doi.org/10.1002/2015GL064097>
- Kropáček, J., Maussion, F., Chen, F., Hoerz, S., & Hochschild, V. (2013). Analysis of ice phenology of lakes on the Tibetan plateau from MODIS data. *The Cryosphere*, *7*(1), 287–301. <https://doi.org/10.5194/tc-7-287-2013>
- Kuang, X., & Jiao, J. J. (2016). Review on climate change on the Tibetan plateau during the last half century. *Journal of Geophysical Research: Atmospheres*, *121*(8), 3979–4007. <https://doi.org/10.1002/2015JD024728>
- Layden, A., Merchant, C., & MacCallum, S. (2015). Global climatology of surface water temperatures of large lakes by remote sensing. *International Journal of Climatology*, *35*(15), 4464–4479. <https://doi.org/10.1002/joc.4299>
- Lazhu, Yang, K., Hou, J., Wang, J., Lei, Y., Zhu, L., et al. (2021). A new finding on the prevalence of rapid water warming during lake ice melting on the Tibetan plateau. *Science Bulletin*, *66*(23), 2358–2361. <https://doi.org/10.1016/j.scib.2021.07.022>
- Lazhu, Yang, K., Wang, J., Lei, Y., Chen, Y., Zhu, L., et al. (2016). Quantifying evaporation and its decadal change for Lake Nam Co, central Tibetan plateau. *Journal of Geophysical Research: Atmospheres*, *121*(13), 7578–7591. <https://doi.org/10.1002/2015JD024523>
- Liu, C., Zhu, L., Wang, J., Ju, J., Ma, Q., Qiao, B., et al. (2021). In-situ water quality investigation of the lakes on the Tibetan plateau. *Science Bulletin*, *66*(17), 1727–1730. <https://doi.org/10.1016/j.scib.2021.04.024>
- Livingstone, D. M., Lotter, A. F., & Kettle, H. (2005). Altitude-dependent differences in the primary physical response of mountain lakes to climatic forcing. *Limnology and Oceanography*, *50*(4), 1313–1325. <https://doi.org/10.4319/lo.2005.50.4.1313>
- Livingstone, D. M., & Padišák, J. (2007). Large-scale coherence in the response of lake surface-water temperatures to synoptic-scale climate forcing during summer. *Limnology and Oceanography*, *52*(2), 896–902. <https://doi.org/10.4319/lo.2007.52.2.0896>
- Ma, Y. (2020). A long-term dataset of integrated land-atmosphere interaction observations on the Tibetan plateau (2005–2016). National Tibetan Plateau Data Center. <https://doi.org/10.11888/Meteoro.tpcd.270910>
- Ma, Y., Hu, Z., Xie, Z., Ma, W., Wang, B., Chen, X., et al. (2020). A long-term (2005–2016) dataset of hourly integrated land-atmosphere interaction observations on the Tibetan plateau. *Earth System Science Data*, *12*(4), 2937–2957. <https://doi.org/10.5194/essd-12-2937-2020>
- MacCallum, S. N., & Merchant, C. J. (2012). Surface water temperature observations of large lakes by optimal estimation. *Canadian Journal of Remote Sensing*, *38*(1), 25–45. <https://doi.org/10.5589/m12-010>
- Magee, M. R., & Wu, C. H. (2017). Response of water temperatures and stratification to changing climate in three lakes with different morphology. *Hydrology and Earth System Sciences*, *21*(12), 6253–6274. <https://doi.org/10.5194/hess-21-6253-2017>

- Magee, M. R., Wu, C. H., Robertson, D. M., Lathrop, R. C., & Hamilton, D. P. (2016). Trends and abrupt changes in 104 years of ice cover and water temperature in a dimictic lake in response to air temperature, wind speed, and water clarity drivers. *Hydrology and Earth System Sciences*, 20(5), 1681–1702. <https://doi.org/10.5194/hess-20-1681-2016>
- Mu, C., Zhang, T., Wu, Q., Peng, X., Zhang, P., Yang, Y., et al. (2016). Dissolved organic carbon, CO<sub>2</sub>, and CH<sub>4</sub> concentrations and their stable isotope ratios in thermokarst lakes on the Qinghai-Tibetan Plateau. *Journal of Limnology*, 75(2), 313–319. <https://doi.org/10.4081/jlimnol.2016.1346>
- Murray, F. W. (1967). On the computation of saturation vapor pressure. *Journal of Applied Meteorology and Climatology*, 6(1), 203–204. [https://doi.org/10.1175/1520-0450\(1967\)006<0203:OTCOSV>2.0.CO;2](https://doi.org/10.1175/1520-0450(1967)006<0203:OTCOSV>2.0.CO;2)
- Niedrist, G. H., Psenner, R., & Sommaruga, R. (2018). Climate warming increases vertical and seasonal water temperature differences and inter-annual variability in a mountain lake. *Climatic Change*, 151(3), 473–490. <https://doi.org/10.1007/s10584-018-2328-6>
- O'Reilly, C. M., Sharma, S., Gray, D. K., Hampton, S. E., Read, J. S., Rowley, R. J., et al. (2015). Rapid and highly variable warming of lake surface waters around the globe. *Geophysical Research Letters*, 42(24), 10773–10781. <https://doi.org/10.1002/2015GL066235>
- Pekel, J.-F., Cottam, A., Gorelick, N., & Belward, A. S. (2016). High-resolution mapping of global surface water and its long-term changes. *Nature*, 540(7633), 418–422. <https://doi.org/10.1038/nature20584>
- Peng, S., Ding, Y., Liu, W., & Li, Z. (2019). 1 km monthly temperature and precipitation dataset for China from 1901 to 2017. *Earth System Science Data*, 11(4), 1931–1946. <https://doi.org/10.5194/essd-11-1931-2019>
- Perroud, M., Goyette, S., Martynov, A., Beniston, M., & Anneville, O. (2009). Simulation of multiannual thermal profiles in deep lake Geneva: A comparison of one-dimensional lake models. *Limnology and Oceanography*, 54(5), 1574–1594. <https://doi.org/10.4319/lo.2009.54.5.1574>
- Piccolroaz, S., Toffolon, M., & Majone, B. (2013). A simple lumped model to convert air temperature into surface water temperature in lakes. *Hydrology and Earth System Sciences*, 17(8), 3323–3338. <https://doi.org/10.5194/hess-17-3323-2013>
- Politi, E., MacCallum, S., Cutler, M. E. J., Merchant, C. J., Rowan, J. S., & Dawson, T. P. (2016). Selection of a network of large lakes and reservoirs suitable for global environmental change analysis using Earth Observation. *International Journal of Remote Sensing*, 37(13), 3042–3060. <https://doi.org/10.1080/01431161.2016.1192702>
- Rao, Y., Liang, S., Wang, D., Yu, Y., Song, Z., Zhou, Y., et al. (2019). Estimating daily average surface air temperature using satellite land surface temperature and top-of-atmosphere radiation products over the Tibetan Plateau. *Remote Sensing of Environment*, 234, 111462. <https://doi.org/10.1016/j.rse.2019.111462>
- Roderick, M. L., Rotstain, L. D., Farquhar, G. D., & Hobbins, M. T. (2007). On the attribution of changing pan evaporation. *Geophysical Research Letters*, 34(17), L7403. <https://doi.org/10.1029/2007GL031166>
- Rose, K. C., Winslow, L. A., Read, J. S., & Hansen, G. J. A. (2016). Climate-induced warming of lakes can be either amplified or suppressed by trends in water clarity. *Limnology and Oceanography Letters*, 1(1), 44–53. <https://doi.org/10.1002/lo.12002>
- Schmid, M., Hunziker, S., & Wüest, A. (2014). Lake surface temperatures in a changing climate: A global sensitivity analysis. *Climatic Change*, 124(1), 301–315. <https://doi.org/10.1007/s10584-014-1087-2>
- Schmid, M., & Köster, O. (2016). Excess warming of a central European lake driven by solar brightening. *Water Resources Research*, 52(10), 8103–8116. <https://doi.org/10.1002/2016WR018651>
- Schneider, P., & Hook, S. J. (2010). Space observations of inland water bodies show rapid surface warming since 1985. *Geophysical Research Letters*, 37(22), L22405. <https://doi.org/10.1029/2010GL045059>
- Sharma, S., Blagrove, K., Magnuson, J. J., O'Reilly, C. M., Oliver, S., Batt, R. D., et al. (2019). Widespread loss of lake ice around the northern hemisphere in a warming world. *Nature Climate Change*, 9(3), 227–231. <https://doi.org/10.1038/s41558-018-0393-5>
- Shimoda, Y., Azim, M. E., Perhar, G., Ramin, M., Kenney, M. A., Sadreddini, S., et al. (2011). Our current understanding of lake ecosystem response to climate change: What have we really learned from the north temperate deep lakes? *Journal of Great Lakes Research*, 37(1), 173–193. <https://doi.org/10.1016/j.jglr.2010.10.004>
- Snortheim, C. A., Hanson, P. C., McMahon, K. D., Read, J. S., Carey, C. C., & Dugan, H. A. (2017). Meteorological drivers of hypolimnetic anoxia in a eutrophic, north temperate lake. *Ecological Modelling*, 343, 39–53. <https://doi.org/10.1016/j.ecolmodel.2016.10.014>
- Song, K., Wang, M., Du, J., Yuan, Y., Ma, J., Wang, M., & Mu, G. (2016). Spatiotemporal variations of lake surface temperature across the Tibetan plateau using MODIS LST product. *Remote Sensing*, 8(10), 854. <https://doi.org/10.3390/rs8100854>
- Stetler, J. T., Girdner, S., Mack, J., Winslow, L. A., Leach, T. H., & Rose, K. C. (2021). Atmospheric stilling and warming air temperatures drive long-term changes in lake stratification in a large oligotrophic lake. *Limnology and Oceanography*, 66(3), 954–964. <https://doi.org/10.1002/lno.11654>
- Su, D., Hu, X., Wen, L., Lyu, S., Gao, X., Zhao, L., et al. (2019). Numerical study on the response of the largest lake in China to climate change. *Hydrology and Earth System Sciences*, 23(4), 2093–2109. <https://doi.org/10.5194/hess-23-2093-2019>
- Subin, Z. M., Riley, W. J., & Mironov, D. (2012). An improved lake model for climate simulations: Model structure, evaluation, and sensitivity analyses in CESM1. *Journal of Advances in Modeling Earth Systems*, 4, M02001. <https://doi.org/10.1029/2011MS000072>
- Tao, S., Fang, J., Ma, S., Cai, Q., Xiong, X., Tian, D., et al. (2020). Changes in China's lakes: Climate and human impacts. *National Science Review*, 7(1), 132–140. <https://doi.org/10.1093/nsr/nwz103>
- Tomlinson, C. J., Chapman, L., Thornes, J. E., & Baker, C. (2011). Remote sensing land surface temperature for meteorology and climatology: A review. *Meteorological Applications*, 18(3), 296–306. <https://doi.org/10.1002/met.287>
- Toms, J. D., & Lesperance, M. L. (2003). Piecewise regression: A tool for identifying ecological thresholds. *Ecology*, 84(8), 2034–2041. <https://doi.org/10.1890/02-0472>
- Tranvik, L. J., Downing, J. A., Cotner, J. B., Loiselle, S. A., Striegl, R. G., Ballatore, T. J., et al. (2009). Lakes and reservoirs as regulators of carbon cycling and climate. *Limnology and Oceanography*, 54, 2298–2314. [https://doi.org/10.4319/lo.2009.54.6\\_part\\_2.2298](https://doi.org/10.4319/lo.2009.54.6_part_2.2298)
- Wan, W., Zhao, L., Xie, H., Liu, B., Li, H., Cui, Y., et al. (2018). Lake surface water temperature change over the Tibetan plateau from 2001 to 2015: A sensitive indicator of the warming climate. *Geophysical Research Letters*, 45(20), 11177–11186. <https://doi.org/10.1029/2018GL078601>
- Wan, Z., Hook, S., & Hulley, G. (2015a). MOD11A1 MODIS/terra land surface temperature/emissivity daily L3 global 1km SIN grid V006. NASA EOSDIS Land Processes DAAC. <https://doi.org/10.5067/MODIS/MOD11A1.006>
- Wan, Z., Hook, S., & Hulley, G. (2015b). MOD11A2 MODIS/terra land surface temperature/emissivity 8-day L3 global 1km SIN grid V006. NASA EOSDIS Land Processes DAAC. <https://doi.org/10.5067/MODIS/MOD11A2.006>
- Wang, B., Ma, Y., Chen, X., Ma, W., Su, Z., & Menenti, M. (2015). Observation and simulation of lake-air heat and water transfer processes in a high-altitude shallow lake on the Tibetan plateau: Plateau lake-air interaction analysis. *Journal of Geophysical Research: Atmospheres*, 120(24), 12327–12344. <https://doi.org/10.1002/2015JD023863>
- Wang, B., Ma, Y., Su, Z., Wang, Y., & Ma, W. (2020). Quantifying the evaporation amounts of 75 high-elevation large dimictic lakes on the Tibetan plateau. *Science Advances*, 6(26), eaay8558. <https://doi.org/10.1126/sciadv.aay8558>

- Wang, B., Ma, Y., Wang, Y., Su, Z., & Ma, W. (2019). Significant differences exist in lake-atmosphere interactions and the evaporation rates of high-elevation small and large lakes. *Journal of Hydrology*, 573, 220–234. <https://doi.org/10.1016/j.jhydrol.2019.03.066>
- Wang, J. (2020). Water temperature observation data at Nam Co lake in Tibet (2011–2014). National Tibetan Plateau Data Center. <https://doi.org/10.11888/Hydro.tpcd.270332>
- Wang, J., Huang, L., Ju, J., Daut, G., Ma, Q., Zhu, L., et al. (2020). Seasonal stratification of a deep, high-altitude, dimictic lake: Nam Co, Tibetan plateau. *Journal of Hydrology*, 584, 124668. <https://doi.org/10.1016/j.jhydrol.2020.124668>
- Wang, J., Huang, L., Ju, J., Daut, G., Wang, Y., Ma, Q., et al. (2019). Spatial and temporal variations in water temperature in a high-altitude deep dimictic mountain lake (Nam Co), central Tibetan Plateau. *Journal of Great Lakes Research*, 45(2), 212–223. <https://doi.org/10.1016/j.jglr.2018.12.005>
- Wang, J., Wang, Q., Zhao, Y., Li, H., Zhai, J., & Shang, Y. (2015). Temporal and spatial characteristics of pan evaporation trends and their attribution to meteorological drivers in the three-river source region, China. *Journal of Geophysical Research: Atmospheres*, 120(13), 6391–6408. <https://doi.org/10.1002/2014JD022874>
- Wang, J., & Wu, G. (2019). Meteorological observation data of Namuco multi circle comprehensive observation and research station (2017–2018). National Tibetan Plateau Data Center. <https://doi.org/10.11888/Meteoro.tpcd.270316>
- Wang, J., Zhu, L., Daut, G., Ju, J., Lin, X., Wang, Y., & Zhen, X. (2009). Investigation of bathymetry and water quality of Lake Nam Co, the largest lake on the central Tibetan plateau, China. *Limnology*, 10(2), 149–158. <https://doi.org/10.1007/s10201-009-0266-8>
- Wang, R., Yang, X., & Zhu, L. (2006). Environmental changes of Namu Co, Xizang during the past 200 years (in Chinese with English abstract). *Quaternary Sciences*, 26(5), 791–798. Retrieved from [http://www.dsjyj.com.cn/article/id/dsjyj\\_8712](http://www.dsjyj.com.cn/article/id/dsjyj_8712)
- Wang, Y., & Wu, G. (2018). Meteorological observation data from the integrated observation and research station of multiple spheres in Namco (2005–2016). National Tibetan Plateau Data Center. <https://doi.org/10.11888/AtmosPhys.tpe.00000049>
- Wen, L., Lv, S., Li, Z., Zhao, L., & Nagabhatla, N. (2015). Impacts of the two biggest lakes on local temperature and precipitation in the yellow river source region of the Tibetan plateau. *Advances in Meteorology*, 248031. <https://doi.org/10.1155/2015/248031>
- Wen, L., Lyu, S., Kirillin, G., Li, Z., & Zhao, L. (2016). Air–lake boundary layer and performance of a simple lake parameterization scheme over the Tibetan highlands. *Tellus A: Dynamic Meteorology and Oceanography*, 68(1), 31091. <https://doi.org/10.3402/tellusa.v68.31091>
- Wilson, R. C., Hook, S. J., Schneider, P., & Schladow, S. G. (2013). Skin and bulk temperature difference at Lake Tahoe: A case study on lake skin effect. *Journal of Geophysical Research: Atmospheres*, 118(18), 10332–10346. <https://doi.org/10.1002/jgrd.50786>
- Winslow, L. A., Leach, T. H., & Rose, K. C. (2018). Global lake response to the recent warming hiatus. *Environmental Research Letters*, 13(5), 054005. <https://doi.org/10.1088/1748-9326/aab9d7>
- Woolway, R. I., Jennings, E., Shatwell, T., Golub, M., Pierson, D. C., & Maberly, S. C. (2021). Lake heatwaves under climate change. *Nature*, 589(7842), 402–407. <https://doi.org/10.1038/s41586-020-03119-1>
- Woolway, R. I., & Merchant, C. J. (2017). Amplified surface temperature response of cold, deep lakes to inter-annual air temperature variability. *Scientific Reports*, 7(1), 4130. <https://doi.org/10.1038/s41598-017-04058-0>
- Woolway, R. I., & Merchant, C. J. (2018). Intralake heterogeneity of thermal responses to climate change: A study of large northern hemisphere lakes. *Journal of Geophysical Research: Atmospheres*, 123(6), 3087–3098. <https://doi.org/10.1002/2017JD027661>
- Woolway, R. I., & Merchant, C. J. (2019). Worldwide alteration of lake mixing regimes in response to climate change. *Nature Geoscience*, 12(4), 271–276. <https://doi.org/10.1038/s41561-019-0322-x>
- Woolway, R. I., Merchant, C. J., Hoek, J. V. D., Azorin-Molina, C., Nöges, P., Laas, A., et al. (2019). Northern hemisphere atmospheric stilling accelerates lake thermal responses to a warming world. *Geophysical Research Letters*, 46(21), 11983–11992. <https://doi.org/10.1029/2019GL082752>
- Wu, Y., Guo, L., Zheng, H., Zhang, B., & Li, M. (2019). Hydroclimate assessment of gridded precipitation products for the Tibetan plateau. *Science of The Total Environment*, 660, 1555–1564. <https://doi.org/10.1016/j.scitotenv.2019.01.119>
- Wu, Y., Huang, A., Lazhu, Yang, X., Qiu, B., Wen, L., et al. (2020). Improvements of the coupled WRF–lake model over Lake Nam Co, central Tibetan plateau. *Climate Dynamics*, 55(9–10), 2703–2724. <https://doi.org/10.1007/s00382-020-05402-3>
- Wu, Y., Huang, A., Lu, Y., Lazhu, Yang, X., Qiu, B., et al. (2021). Numerical study of the thermal structure and circulation in a large and deep dimictic lake over Tibetan plateau. *Journal of Geophysical Research: Oceans*, 126(10), e2021JC017517. <https://doi.org/10.1029/2021JC017517>
- Wu, Y., Huang, A., Yang, B., Dong, G., Wen, L., Lazhu, et al. (2019). Numerical study on the climatic effect of the lake clusters over Tibetan plateau in summer. *Climate Dynamics*, 53(9), 5215–5236. <https://doi.org/10.1007/s00382-019-04856-4>
- Wu, Y., & Zhu, L. (2008). The response of lake–glacier variations to climate change in Nam Co catchment, central Tibetan plateau, during 1970–2000. *Journal of Geographical Sciences*, 18(2), 177–189. <https://doi.org/10.1007/s11442-008-0177-3>
- Xu, L., Liu, H., Du, Q., & Wang, L. (2016). Evaluation of the WRF–lake model over a highland freshwater lake in southwest China: Evaluation of the WRF–lake model. *Journal of Geophysical Research: Atmospheres*, 121(23), 13989–14005. <https://doi.org/10.1002/2016JD025396>
- Xu, X., Lu, C., Shi, X., & Gao, S. (2008). World water tower: An atmospheric perspective. *Geophysical Research Letters*, 35(20), L20815. <https://doi.org/10.1029/2008GL035867>
- Yan, F., Sillanpää, M., Kang, S., Aho, K. S., Qu, B., Wei, D., et al. (2018). Lakes on the Tibetan plateau as conduits of greenhouse gases to the atmosphere. *Journal of Geophysical Research: Biogeosciences*, 123(7), 2091–2103. <https://doi.org/10.1029/2017JG004379>
- Yan, Y., Liu, X., Wen, Y., & Ou, J. (2019). Quantitative analysis of the contributions of climatic and human factors to grassland productivity in northern China. *Ecological Indicators*, 103, 542–553. <https://doi.org/10.1016/j.ecolind.2019.04.020>
- Yang, K., Ding, B., Qin, J., Tang, W., Lu, N., & Lin, C. (2012). Can aerosol loading explain the solar dimming over the Tibetan plateau? *Geophysical Research Letters*, 39(20), L20710. <https://doi.org/10.1029/2012GL053733>
- Yang, K., & He, J. (2019). China meteorological forcing dataset (1979–2018). National Tibetan Plateau Data Center. <https://doi.org/10.11888/AtmosphericPhysics.tpe.249369.file>
- Yang, K., Wu, H., Qin, J., Lin, C., Tang, W., & Chen, Y. (2014). Recent climate changes over the Tibetan plateau and their impacts on energy and water cycle: A review. *Global and Planetary Change*, 112, 79–91. <https://doi.org/10.1016/j.gloplacha.2013.12.001>
- Yang, K., Yu, Z., & Luo, Y. (2020). Analysis on driving factors of lake surface water temperature for major lakes in Yunnan–Guizhou plateau. *Water Research*, 184, 116018. <https://doi.org/10.1016/j.watres.2020.116018>
- Ying, L., Shen, Z., & Piao, S. (2015). The recent hiatus in global warming of the land surface: Scale-dependent breakpoint occurrences in space and time. *Geophysical Research Letters*, 42(15), 6471–6478. <https://doi.org/10.1002/2015GL064884>
- You, Q., Kang, S., Li, C., Li, M., & Liu, J. (2007). Variation features of meteorological elements at Namco station, Tibetan plateau (in Chinese with English abstract). *Meteorological*, 33(3), 54–60. Retrieved from <http://qxqk.nmc.cn/html/2007/3/20070308.html>
- Zhang, G., Luo, W., Chen, W., & Zheng, G. (2019). A robust but variable lake expansion on the Tibetan plateau. *Science Bulletin*, 64(18), 1306–1309. <https://doi.org/10.1016/j.scib.2019.07.018>

- Zhang, G., Yao, T., Piao, S., Bolch, T., Xie, H., Chen, D., et al. (2017). Extensive and drastically different alpine lake changes on Asia's high plateaus during the past four decades. *Geophysical Research Letters*, *44*(1), 252–260. <https://doi.org/10.1002/2016GL072033>
- Zhang, G., Yao, T., Xie, H., Qin, J., Ye, Q., Dai, Y., & Guo, R. (2014). Estimating surface temperature changes of lakes in the Tibetan plateau using MODIS LST data. *Journal of Geophysical Research: Atmospheres*, *119*(14), 8552–8567. <https://doi.org/10.1002/2014JD021615>
- Zhang, G., Yao, T., Xie, H., Yang, K., Zhu, L., Shum, C. K., et al. (2020). Response of Tibetan plateau lakes to climate change: Trends, patterns, and mechanisms. *Earth-Science Reviews*, *208*, 103269. <https://doi.org/10.1016/j.earscirev.2020.103269>
- Zhang, R., Chan, S., Bindlish, R., & Lakshmi, V. (2021). Evaluation of global surface water temperature data sets for use in passive remote sensing of soil moisture. *Remote Sensing*, *13*(10), 1872. <https://doi.org/10.3390/rs13101872>
- Zhao, G., Gao, H., & Cai, X. (2020). Estimating lake temperature profile and evaporation losses by leveraging MODIS LST data. *Remote Sensing of Environment*, *251*, 112104. <https://doi.org/10.1016/j.rse.2020.112104>
- Zhong, Y., Notaro, M., Vavrus, S. J., & Foster, M. J. (2016). Recent accelerated warming of the Laurentian great lakes: Physical drivers. *Limnology and Oceanography*, *61*(5), 1762–1786. <https://doi.org/10.1002/lno.10331>
- Zhu, L., Xie, M., & Wu, Y. (2010). Quantitative analysis of lake area variations and the influence factors from 1971 to 2004 in the Nam Co basin of the Tibetan plateau. *Chinese Science Bulletin*, *55*(13), 1294–1303. <https://doi.org/10.1007/s11434-010-0015-8>